Cluster observations of the midaltitude cusp under strong northward interplanetary magnetic field

R. Hu,[1,2,3] Y. V. Bogdanova,[1,4] C. J. Owen,[1] C. Foullon,[1] A. N. Fazakerley,[1] and H. Rème[5]

Received 10 August 2007; revised 31 January 2008; accepted 17 March 2008; published 22 July 2008.

[1] We report on a multispacecraft cusp observation lasting more than 100 min. We determine the cusp boundary motion and reveal the effect on the cusp size of the interplanetary magnetic field (IMF) changing from southward to northward. The cusp shrinks at the beginning of the IMF rotation and it reexpands at the rate of 0.40° invariant latitude per hour under stable northward IMF. On the basis of plasma signatures inside the cusp, such as counterstreaming electrons with balanced fluxes, we propose that pulsed dual lobe reconnection operates during the time of interest. SC1 and SC4 observations suggest a long-term regular periodicity of the pulsed dual reconnection, which we estimate to be ~1–5 min. Further, the distances from the spacecraft to the reconnection site are estimated on the basis of observations from three satellites. The distance determined using SC1 and SC4 observations is ~15 R_E and that determined from SC3 data is ~8 R_E. The large-scale speed of the reconnection site sunward motion is ~16 km s^{-1}. We observe also a fast motion of the reconnection site by SC1, which provides new information about the transitional phase after the IMF rotation. Finally, a statistical study of the dependency of plasma convection inside the cusp on the IMF clock angle is performed. The relationship between the cusp stagnation, the dual lobe reconnection process, and the IMF clock angle is discussed.

Citation: Hu, R., Y. V. Bogdanova, C. J. Owen, C. Foullon, A. N. Fazakerley, and H. Rème (2008), Cluster observations of the midaltitude cusp under strong northward interplanetary magnetic field, *J. Geophys. Res.*, *113*, A07S05, doi:10.1029/2007JA012726.

1. Introduction

[2] The cusp regions are null points in the magnetic field above the southern and northern poles and are populated by magnetosheath-like plasma with specific particle signatures. It is now believed that the most common process responsible for the magnetosheath plasma penetration into the magnetosphere is magnetic reconnection. During reconnection between terrestrial magnetic field lines and the interplanetary magnetic field (IMF) lines, new field lines with one end at the Earth and the other end in the interplanetary medium are created. Thus, along such field lines, the solar wind plasma may penetrate into the Earth's magnetosphere. It is known that reconnection is more likely to happen at the dayside magnetopause near the subsolar point during southward IMF [*Dungey*, 1961], or at locations where the shear between terrestrial field lines and IMF is very large.

[3] During northward IMF, reconnection is more likely to occur poleward of the cusp region, in the lobe sector of the magnetopause [*Dungey*, 1963; *Crooker*, 1979]. The signatures of lobe reconnection in cusp observations are: injections of particles at the poleward edge of the cusp; an inverse energy-latitude dispersion in the ion energy-time spectrogram, i.e., the energy of the injected particles increases with increasing latitude; an inverse low-energy ion cutoff observed near the poleward boundary of the cusp [e.g., *Reiff et al.*, 1980; *Burch et al.*, 1980]; and sunward convection inside the cusp [e.g., *Smith and Lockwood*, 1996]. The cusp formed because of lobe reconnection has often been observed during northward IMF [e.g., *Fuselier et al.* , 2000a, 2000b; *Twitty et al.*, 2004; *Trattner et al.*, 2004; *Lavraud et al.*, 2005; *Bogdanova et al.*, 2005].

[4] Moreover, it was suggested that during northward IMF, dual lobe reconnection might take place [e.g., *Song and Russell*, 1992]. During dual lobe reconnection, the open field lines of lobes in both hemispheres reconnect poleward of the cusps with the magnetosheath field lines, thus creating newly closed field lines with magnetosheath plasma captured inside them. The signatures of dual lobe reconnection have been reported in the magnetosheath boundary layer [e.g., *Onsager et al.*, 2001; *Lavraud et al.*, 2006], inside the cusp region at midaltitudes [*Fuselier et al.*, 2001; *Bogdanova et al.*, 2005] and inside the cusp region in the ionosphere [*Sandholt et al.*, 2000; *Provan et al.*, 2005; *Imber et al.*, 2006]. It has been suggested that signatures of dual lobe reconnection outside the magnetosphere, in the

[1]Mullard Space Science Laboratory, University College London, Dorking, UK.
[2]Ecole Centrale Paris, Paris, France.
[3]Now at Tsinghua Centre for Astrophysics, Department of Physics, Tsinghua University, Beijing, China.
[4]Now at Department of Physics, La Trobe University, Melbourne, Victoria, Australia.
[5]Centre d'Etude Spatiale des Rayonnements, Centre National de la Recherche Scientifique, Toulouse, France.

0148-0227/08/2007JA012726

magnetosheath boundary layer, are bidirectional electron beams [e.g., *Onsager et al.*, 2001; *Lavraud et al.*, 2006]. Inside the magnetosphere, a number of signatures have been suggested as features of the reclosed field line configuration. Inside the boundary layers the signatures are: (1) the existence of a trapped high-energy plasma sheet population alongside the accelerated magnetosheath-like population and (2) bidirectional electron beams at magnetosheath-like energies with equal fluxes at all energies in the parallel and antiparallel directions [e.g., *Phan et al.*, 2005].

[5] Inside the cusp region, the signatures of reclosed field lines are (1) a downgoing oxygen population [*Fuselier et al.*, 2001], which might be explained by the ion outflow from the opposite hemisphere (however, such a population is rarely observed because of a large travel time); (2) accelerated plasma population with energies higher than inside the typical cusp, which might be explained by the additional plasma acceleration at the second reconnection site [e.g., *Onsager et al.*, 2001; *Bogdanova et al.*, 2005]; and (3) an isotropic plasma population, which might be explained by pitch angle scattering of the ion and electron populations on field lines with a long history since reconnection [*Bogdanova et al.*, 2005]. There are various suggestions about the expected plasma convection signatures inside the cusp, which correspond to dual lobe reconnection. *Bogdanova et al.* [2005] proposed that plasma observed on closed field lines may be almost stagnant, as these field lines are disconnected from the solar wind driver. Conversely, *Provan et al.* [2005] and *Imber et al.* [2006] suggested that the process of dual lobe reconnection may be accompanied by a strong sunward convection of plasma. However, convection of reclosed field lines might be more complicated: at the beginning, when a field line just undergoes reconnection in the second hemisphere, some sunward convection might be observed. Later, when the reclosed field line ''sinks'' inside the magnetosphere, the convection is expected to become nearly stagnant. Thus, we suppose that previous studies deal with different ''stages'' of the lifetime of reclosed field lines. These studies based their conclusions on an investigation of single events. Thus, a wider sample of events needs to be studied in order to understand plasma convection inside the cusp driven by dual lobe reconnection.

[6] The IMF conditions which are favorable for dual lobe reconnection to occur is another area of active debate. On the basis of ionospheric observations, *Imber et al.* [2006] suggested that dual lobe reconnection might occur only under very strong northward IMF with the magnitude of the clock angle less than 10°. Here, the IMF clock angle is defined as $CA = \tan^{-1}(B_Y/B_Z)$ where B_Y and B_Z are components in the GSM coordinate system. However, on the basis of observations of bidirectional electron beams in the magnetosheath, *Lavraud et al.* [2006] performed a statistical study which showed that dual lobe reconnection might occur under IMF clock angles in the range $\pm(0-40°)$. Throughout the paper, we will refer to the clock angle magnitude when we speak about the clock angle.

[7] Thus, there is ambiguity in (1) the plasma convection signatures inside the cusp region corresponding to the dual lobe reconnection and (2) the IMF conditions favorable for the dual lobe reconnection. The aim of the present work is to try to address these two questions. To do this, we studied midaltitude cusp crossings by Cluster under northward IMF with different clock angles. We found only one event during 1 year of observations (2002) when Cluster crossed the midaltitude cusp region under very strong northward IMF with clock angle <10°. We first studied this event in depth to find unambiguous evidence of the signatures of dual lobe reconnection, assuming that for such IMF conditions dual lobe reconnection does indeed occur. Then we performed analysis of the plasma convection inside the midaltitude cusp region under different clock angles to see if the slow convection inside the cusp is observed for lower clock angles and thus might indicate the occurrence of dual lobe reconnection.

[8] This manuscript is organized as follows: section 2 gives a brief description of the Cluster and ACE missions and the instruments used in this study, section 3 presents Cluster multispacecraft observations of one event under strong northward IMF, section 4 contains discussion of this event, section 5 presents results of statistical study of the plasma convection inside the cusp, and finally section 6 gives the conclusions.

2. Cluster and ACE Satellites and Instrumentation

[9] This study uses data from the Cluster satellites inside the cusp. The Cluster orbit has a perigee of ~4 R_E, an apogee of ~19.7 R_E, an inclination of ~90°, and an orbital period of ~57 h [*Escoubet et al.*, 2001]. The observations reported here were acquired by the Plasma Electron and Current Experiment (PEACE) [*Johnstone et al.*, 1997], as well as by the Hot Ion Analyzer (HIA) and Composition and Distribution Function (CODIF) sensors, which are parts of the Cluster Ion Spectrometer (CIS) experiment [*Rème et al.*, 2001]. These instruments are mounted on each of the 4 Cluster satellites. The HIA sensor employs an electrostatic analyzer (ESA) to measure ions of all species with high angular and high-energy resolution. The CODIF sensor combines a top hat analyzer with an instantaneous 360° field of view, with a time of flight section to measure the complete 3-D distribution functions of the major ion species, H^+, He^{++}, He^+, and O^+. The sensor covers the energy range between 0.02 and 38 keV/q with a time resolution of 4 s. Each PEACE package consists of two sensors, the HEEA (High-Energy Electron Analyzer) and the LEEA (Low-Energy Electron Analyzer), mounted on diametrically opposite sides of the spacecraft. They are designed to measure the 3-D velocity distributions of electrons in the range of 0.6 eV to ~26 keV, with a time resolution of 4 s. The spacecraft potential was measured by the Electric Fields and Waves (EFW) instrument [*Gustafsson et al.*, 2001]. We also used magnetic field data from the Fluxgate Magnetometer (FGM) [*Balogh et al.*, 2001] with 4 s resolution.

[10] The solar wind and IMF conditions were monitored by the ACE spacecraft. ACE orbits the L1 libration point, a point of Earth-Sun gravitational equilibrium, about 1.5 million km from Earth and 148.5 million km from the Sun. The interplanetary magnetic field data came from the Magnetic Field Experiment (MAG) [*Smith et al.*, 1998]. The solar wind density and velocity came from the Solar Wind Electron

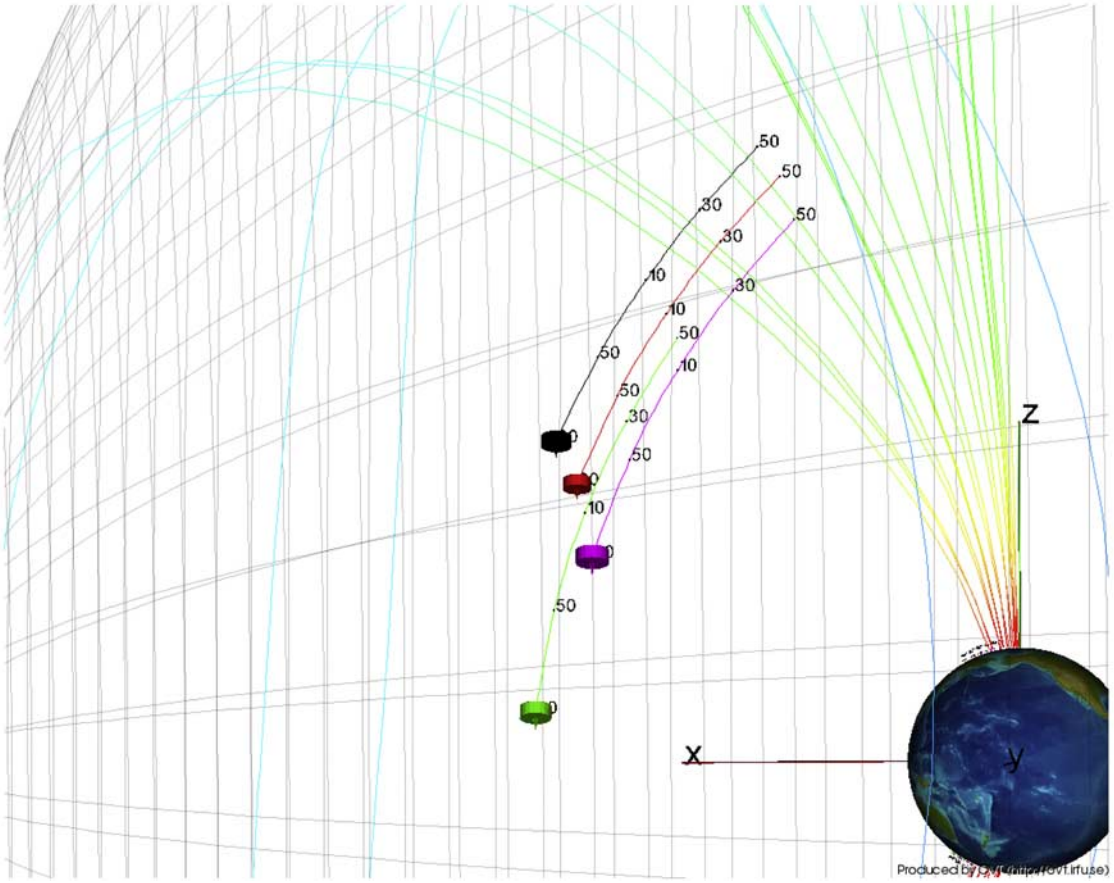

Figure 1. Orbits of Cluster satellites in the GSM *X-Z* plane during the period 0430–0600 UT. The black line shows the orbit of SC1, the red line shows the orbit of SC2, the green line shows the orbit of SC3, and the magenta line shows the orbit of SC4. The symbols of the spacecraft show their positions at 0430 UT. Magnetic field lines are shown for illustration only.

Proton Alpha Monitor (SWEPAM) [*McComas et al.*, 1998]. The time lag associated with solar wind convection between the ACE and Cluster observations inside the cusp was calculated on the basis of the *X* component of the solar wind velocity in the GSE coordinate system (measured with a resolution of 64 s) and the position of ACE along Sun-Earth line (GSE *X* axis).

3. Observations of the Midaltitude Cusp Crossing During Strong Northward IMF

3.1. Cluster Orbit, IMF, and Solar Wind Conditions

[11] During September 2002 the Cluster satellites crossed the midaltitude cusp region in the string-of-pearls configuration. In this formation, Cluster SC3 is separated from the other three spacecraft by up to ~2.5 R_E when it is inside the midaltitude cusp and polar cap. On 8 September 2002 during the period ~0450–0640 UT, the Cluster satellites cross the northern cusp region. The orbits of four Cluster satellites moving from low to high latitudes via the cusp are shown in Figure 1, with SC1 indicated by black, SC2 by red, SC3 by green, and SC4 by magenta. The order of the passage through the cusp is SC1, SC2, SC4, and SC3. In this paper we will concentrate on observations from SC1, SC3, and SC4 in order to explore the full data set available from these three satellites.

[12] The IMF and the solar wind (SW) conditions, observed by the ACE spacecraft between 0450 and 0640 UT, are shown in Figure 2. Figures 2a–2c show the GSM *X*, *Y*, and *Z* components of the IMF; Figure 2d shows the clock angle (CA) of the IMF; Figure 2e presents the H^+ density of the solar wind; Figure 2f shows the bulk speed of the solar wind; and the Figure 2g shows the dynamic pressure of the solar wind. The time series are shifted forward by 55 min. This propagation delay is estimated by taking into account the *X* component of the solar wind velocity, 460–480 km s^{-1} during the event and the *X* GSE location of the ACE satellite. This time lag is consistent with the time lag calculated using a recent method discussed by *Weimer et al.* [2003]. The eight vertical dashed lines correspond to the times when each Cluster satellite enters and leaves the cusp region.

[13] At the beginning of the interval of interest, when SC1 and SC2 enter the cusp, the IMF is southward ($B_Z \sim -5$ to -10 nT) and largely duskward ($B_Y \sim 5$–10 nT). From ~0457 to ~0503 UT, the solar wind dynamic pressure increases from 4 to 8 nPa, and the IMF turns northward then remains strongly northward ($B_Z \sim 8$–10 nT) until the end of

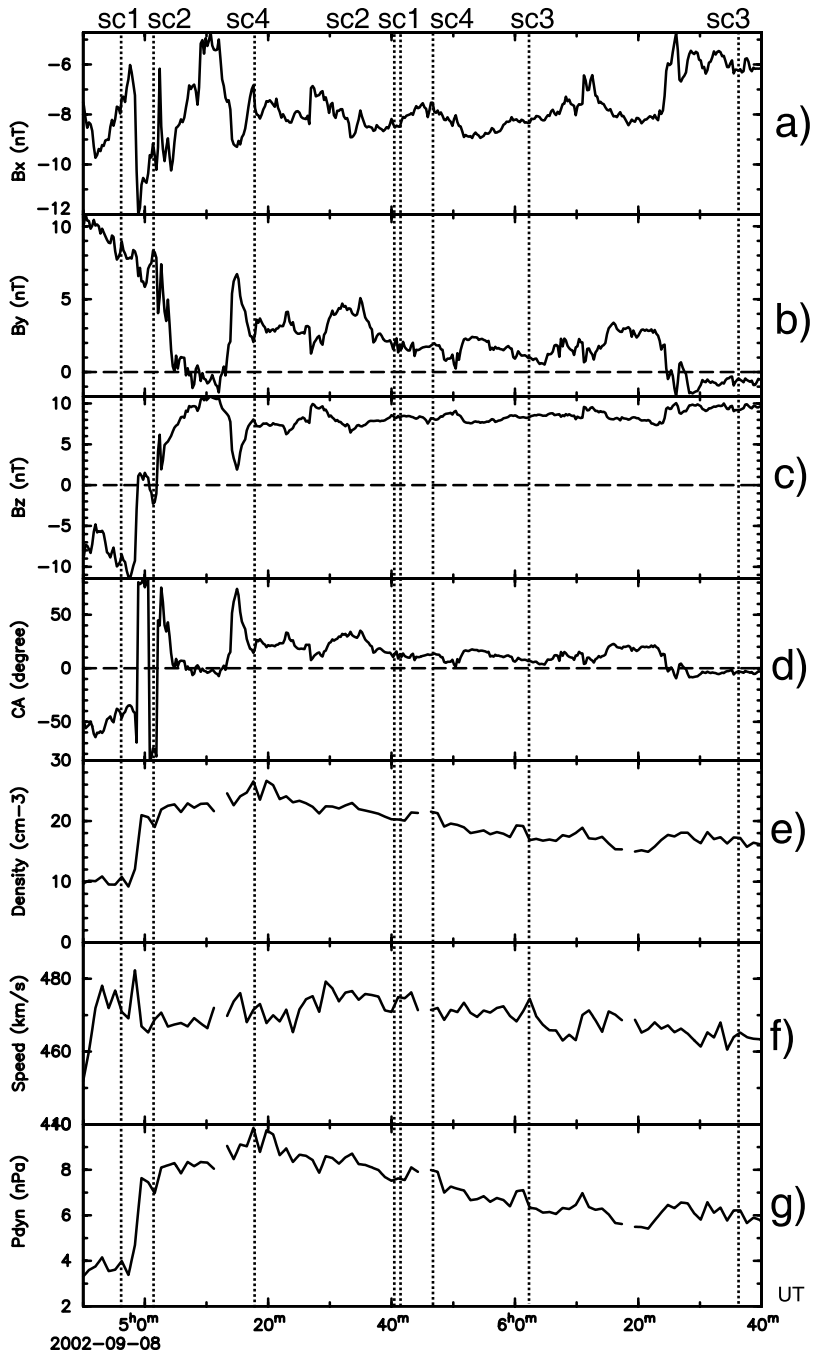

Figure 2. The IMF and solar wind conditions measured by ACE satellite on 8 September 2002 from 0450 to 0640 UT. The time series are lagged by 55 min taking into account the solar wind propagation time. (a–c) The GSM *X*, *Y*, and *Z* components of the interplanetary magnetic field. (d) The calculated IMF clock angle. (e and f) The solar wind plasma density and bulk velocity, respectively. (g) The calculated solar wind dynamic pressure. The vertical dashed lines show the time when each spacecraft enters and leaves the cusp.

the period of interest, when SC4 and SC3 enter and leave the cusp region. The density of the solar wind reaches its highest value, 27 cm^{-3} at ~0520 UT, then gradually decreases and returns to a stable value of 16 cm^{-3}. The solar wind pressure also reaches its highest value of 10 nPa at ~0520 UT. The IMF is due northward, CA ~0°, from ~0505 to ~0513 UT; from ~0517 UT the IMF CA remains $<\pm 20°$. For the whole period, the IMF B_X component is negative; this favors the occurrence of reconnection in the northern lobe sector (summer hemisphere).

[14] In the next section we report the data from SC1, SC4, and SC3, in this order the satellites crossing successively the cusp, and report in detail the azimuthal cuts through the electron energy spectra and ion phase space density distributions for the selected times. Further

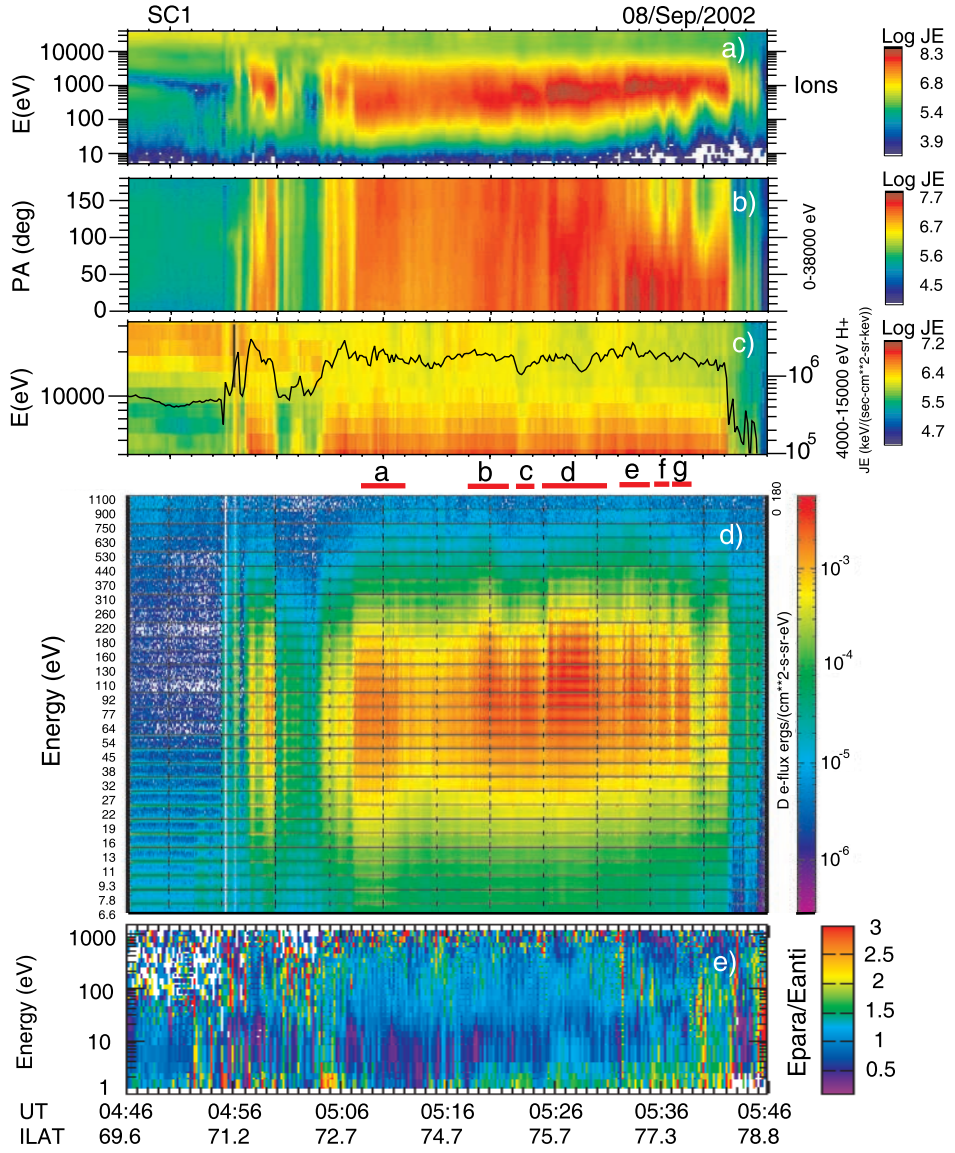

Figure 3. Electron and ion data based on the CIS-HIA and PEACE LEEA observations on SC1 on 8 September 2002 from 0446 to 0546 UT. (a and b) The ion energy-time spectrogram and pitch angle distribution measured by the CIS-HIA instrument. The whole energy range of the instrument has been used. Differential energy flux is color coded. (c) The energy-time spectrogram of the ions for the high-energy population only, $E = 4–32$ keV (corresponding scale on the left). Differential energy flux is color coded. The over-plotted black line represents the integrated energy flux of ions with energies $E = 4–15$ keV (corresponding scale on the right). (d) Consists of 30 sections, where each section shows the electron pitch angle spectrogram for an energy range indicated on the left. The 4 s data from the PEACE LEEA sensor have been used and was corrected for the photoelectron population. Differential energy flux is color coded. (e) Energy-time plot where the anisotropy of the counterstreaming electron population is color coded. The color represents the ratio of the differential energy flux of the population moving parallel to the magnetic field to the differential energy flux of the population moving antiparallel to the magnetic field. Below the plot, the universal time and corresponding invariant latitude are indicated. The short red bold lines in the middle indicate times of separate electron beams a–g discussed in the text.

discussion will be in the GSM coordinate system unless otherwise stated.

3.2. Cusp Crossing Observations by Cluster 1

[15] An overview of SC1 plasma data is shown in Figures 3 and 4. Figure 3 presents electron and ion data based on the CIS-HIA and PEACE LEEA sensor observations on 8 September 2002 from 0446 to 0546 UT. Figures 3a and 3b present the ion energy-time spectrogram and pitch angle distribution measured by CIS-HIA instrument. The whole energy range of the instrument has been used for Figures 3a and 3b. Differential energy flux is

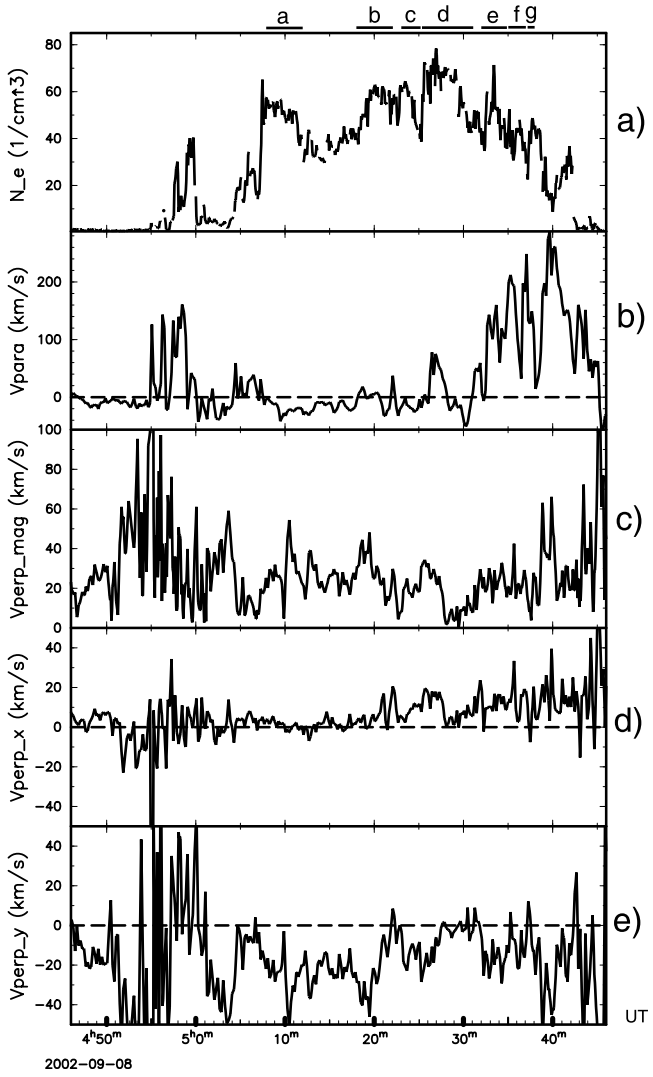

Figure 4. The plasma parameters calculated on the basis of the PEACE and CIS-HIA observations on SC1 on 8 September 2002 from 0446 to 0546 UT. (a) The electron density and (b–e) the ion bulk velocity in the magnetic field-aligned coordinate system: the parallel velocity (Figure 4b), the magnitude of the convection (perpendicular) velocity (Figure 4c), and the X and Y components of the perpendicular velocity (Figures 4d and 4e, respectively). The GSM coordinate system has been used for the velocity components. The short bold lines above the plot indicate times corresponding to a separate electron beams a–g discussed in the text.

color coded. Figure 3c shows the energy-time spectrogram of the ions for the high-energy population only, $E = 4–32$ keV (corresponding scale on the left). Differential energy flux is color coded. The over-plotted black line represents the integrated energy flux of ions with energies $E = 4–15$ keV (corresponding scale on the right). This limited energy range is used in order to include the accelerated magnetosheath population and exclude the plasma sheet population. Figure 3d consists of 30 sections, where each section shows the electron pitch angle spectrogram for an energy range indicated on the left. The 4 s data from the PEACE LEEA sensor have been used. The spacecraft potential has been used to eliminate photoelectrons, and the energy of the population has been corrected for this effect. Differential energy flux is color coded. Figure 3e is an energy-time plot where the anisotropy of the counterstreaming electron population is color coded. The color represents the ratio of the differential energy flux of the population moving parallel to the magnetic field to the differential energy flux of the population moving antiparallel to the magnetic field. Below the plot, the universal time and corresponding invariant latitude are indicated. The short bold lines it the middle indicate the times of the separate electron beams a–g discussed in the text.

[16] Figure 4 shows the plasma moments calculated on the basis of the PEACE and CIS-HIA observations on SC1 on 8 September 2002 from 0446 to 0546 UT. Figure 4a presents the electron density and Figures 4b–4e show the ion bulk velocity in the magnetic field-aligned coordinate system: the velocity parallel to the magnetic field (Figure 4b), the magnitude of the convection (perpendicular to the magnetic field) velocity (Figure 4c), the X and Y components of the perpendicular velocity (Figures 4d and 4e, respectively). The GSM coordinate system has been used for the velocity components. The short bold lines above the plot indicate the times corresponding to the separate electron beams a–g discussed in the text. We use the ion velocity perpendicular to the magnetic field lines to demonstrate the motion of the field lines, because of the validity of "frozen in" conditions. Therefore we consider only the perpendicular velocity for the plasma convection further in this paper.

[17] From ~0456 UT SC1 begins to detect magnetosheath-like plasma, e.g., ions with energy in the range 100 eV–6 keV (Figure 3). From ~0457 to ~0500 UT the spacecraft detects a significant flux enhancement of both electrons and ions. During this period we observe three short durations separated electron beams whose energy ranges from 14 to 270 eV, at ~0457, ~0459, and ~0500 UT. Both downgoing and upgoing populations are seen, while the upgoing population (pitch angle 180°) seems to dominate the low-energy (~9.6 eV) and high-energy (~290 eV) bands. Further, the ion spectrogram (Figure 3a) shows the low-energy cutoff decrease with time and latitude, which is expected during dayside reconnection events [e.g., *Smith and Lockwood*, 1996]. The ions are observed over an energy range from 300 eV to 4 keV, while at ~0500 UT, they appear over an energy range from 200 eV to 3 keV. During this time, the ion parallel velocity is positive, with magnitude up to 100 km s^{-1}, which indicates a significant downward ion injection. Meanwhile, the perpendicular velocity (Figures 4d and 4e) shows duskward convection, and the sunward-antisunward component of the convection is highly variable.

[18] From ~0500 to ~0504 UT, the high-density population disappears except for one weak beam which is seen at ~0501 UT. At this time plasma sheet ions are evident. However, the electrons are still of magnetosheath origin, with energies 9.3–260 eV. Such plasma characteristics are typical for the electron edge of the low-latitude boundary layer [*Bogdanova et al.*, 2006]. We note that these variations in plasma parameters appear when the solar wind dynamic pressure strongly increases, and thus it might be a spatial rather than temporal variation of the plasma parameters.

[19] Later, the electron density increases quickly from 20 cm^{-3} at ~0504 UT to 60 cm^{-3} at ~0507 UT. From ~0504 to ~0508 UT, the electron and ions distributions show also an energy-latitude dispersion decreasing with latitude, indicating that these populations may surely be on field lines which have undergone dayside reconnection. From ~0508 to ~0542 UT, we observe seven separate strong electron beams (Figure 3d) which correspond to the peaks of the electron density as shown in Figure 4, at 0508–0512 UT (beam a), 0518–0522 UT (beam b), 0523–0525 UT (beam c), 0525–0531 UT (beam d), 0532–0535 UT (beam e), 0535–0537 UT (beam f), and 0537–0538 UT (beam g). These separate electron beams, which might be identified as separate variations in the electron energy, flux and density, are indicated by bold horizontal lines in the middle of Figure 3 and on the top of Figure 4.

[20] There are other electron populations apart from these beams, but with lower-energy flux and density. Beam d has the highest density (Figure 4a). Beam a has electron energy from ~9.6 to ~290 eV (Figure 3d). Significant fluxes of high-energy (~340 eV) population are observed in beams b, d, e, f, and g. We note that beams b, d, and e seem to be bidirectional in all energy channels, including the high-energy end, while the upgoing population dominates the high-energy end of beams f and g. Equal fluxes of the counterstreaming population during beams b, d, and e and dominant upgoing population at high energies during beams f and g also can be seen in Figure 3e. In Figure 3e, if we compare the ratio of parallel fluxes and antiparallel fluxes during the electron beams and near the cusp equatorward and poleward boundary, it is clear that the electron beams are more balanced. Beam c does not have a population in the 340 eV band, but it seems to be bidirectional in all energy channels. From ~0530 UT, the low-energy cutoffs of the beams increase with latitude, which indicates lobe reconnection events [*Reiff et al.*, 1980; *Burch et al.*, 1980; *Twitty et al.*, 2004].

[21] We now look into the ion spectrogram and convection during the same time period. From ~0508 to ~0542 UT, we observe a general inverse ion low-energy cutoff, e.g., the ion low-energy cutoff is increasing with latitude (or, in our case, time) in the ion spectrogram (Figure 3a), which is consistent with lobe reconnection. Some short-scale decreases of the low-energy cutoff are observed from ~0530 UT. This may relate to the motion of the cusp, or to the separate plasma injections in the cusp [*Lockwood and Smith*, 1994]. Investigating only the high-energy part of the ion population (Figure 3c), we observe enhanced fluxes of high-energy ions ($E > 4$ keV) at 0456–0500 UT, 0505–0512 UT (including the time interval of beam a), 0517–0523 UT (around the time of beam b), 0524–0528 UT (beams c and d), and 0530–0542 UT (beams d, e, f, and g). We note that the enhancements of high-energy ion fluxes, $E = 4$–15 keV, generally correlate with the electron beams taking into account the fact that the ions and electrons have different travel times. Moreover, during some short time intervals, enhancements of the fluxes of ions with plasma sheet energies, $E = 20$–38 keV, are detected.

[22] From ~0507 to ~0532 UT (beams a, b, c, and d), the pitch angle distribution of ions remains isotropic. During this time interval the parallel velocity is low, $V_{para} \sim -0$–40 km s^{-1}, which corresponds to domination of the upflowing population. However, during the small time intervals inside beams b, c, and d, the parallel velocity becomes positive, $V_{para} = 0$–40 km s^{-1}, indicating domination of plasma injections. During the time interval 0507–0532 UT, the perpendicular velocity is relatively small ($|V_{perp}| < 40$ km s^{-1}). Plasma convection in the sunward-antisunward direction is very low, $V_{perp\_x} \sim 0$–20 km s^{-1}, while stronger convection is observed toward dawn, $V_{perp\_y} \sim -0$–40 km s^{-1}. We consider this region to be a region with reduced convection because much lower convection speeds are observed in comparison with the convection detected near the cusp poleward boundary. Thus, from ~0532 UT, the plasma moves significantly sunward and dawnward, with $V_{perp\_x} \sim 20$–40 and $V_{perp\_y} \sim -0$–60 km s^{-1}. From ~0532 to ~0542 UT, downgoing ion injections dominate, except for short periods around 0536 (beam f) and 0538 UT (beam g), where the isotropic distribution reappears. Very high parallel velocities (Figure 4b) also indicate ion injections from ~0532 UT, with V_{para} up to 300 km s^{-1}. We note that this downgoing injection appears at the poleward boundary of the cusp, which is consistent with the lobe reconnection process. After ~0542 UT, before entering the polar cap, the spacecraft detects low fluxes of magnetosheath-like ions and electrons. This might indicate some boundary layer population.

[23] To summarize, SC1 enters the cusp when the IMF changes orientation from southward to northward. The spacecraft detects a region with reduced convection in the middle of the cusp and plasma injections with inverse low-energy cutoff near the poleward boundary of the cusp, which is consistent with lobe reconnection. Several separate electron beams are observed, and some of them are bidirectional at all energies. On the cusp equatorward boundary, a short-term separate population consistent with dayside reconnection is observed. We will discuss these plasma properties later on in the paper.

3.3. Cusp Crossing Observations by Cluster 4

[24] An overview of the SC4 plasma data is shown in Figures 5 and 6 whose formats are similar to Figures 3 and 4, respectively. However, for the analysis of ion data we used observations of the H^+ ion population from the CIS-CODIF instrument, as the HIA instrument does not work on SC4. In this case we use high-resolution ground-calculated 3-D moments to produce the electron density shown in Figure 6 since the PEACE instrument is in burst mode on SC4.

[25] From ~0519 UT SC4 begins to detect magnetosheath-like plasma about 16 min after SC1. In both electron and H^+ spectrograms we can see clear sharp equatorward and poleward boundaries of the cusp, at ~0521 and ~0546 UT, respectively. During this cusp crossing, many electron beams are seen, and some of them are bidirectional in all energy channels. Before ~0530 UT, the electron energy ranges from 14 to 220 eV. From ~0530 UT, higher-energy electrons (about 280 eV) are detected as well, and the lower-energy (about 14 and 19 eV) population declines. After ~0530 UT we observe four electron beams, at 0530–0534 UT (beam h), 0534–0535 UT (beam i), 0537–0538 UT (beam j), and ~0543 UT (beam k), with high-energy and bidirectional fluxes, which suggest that these beams may be due to dual lobe reconnection [*Phan et al.*, 2005]. On the

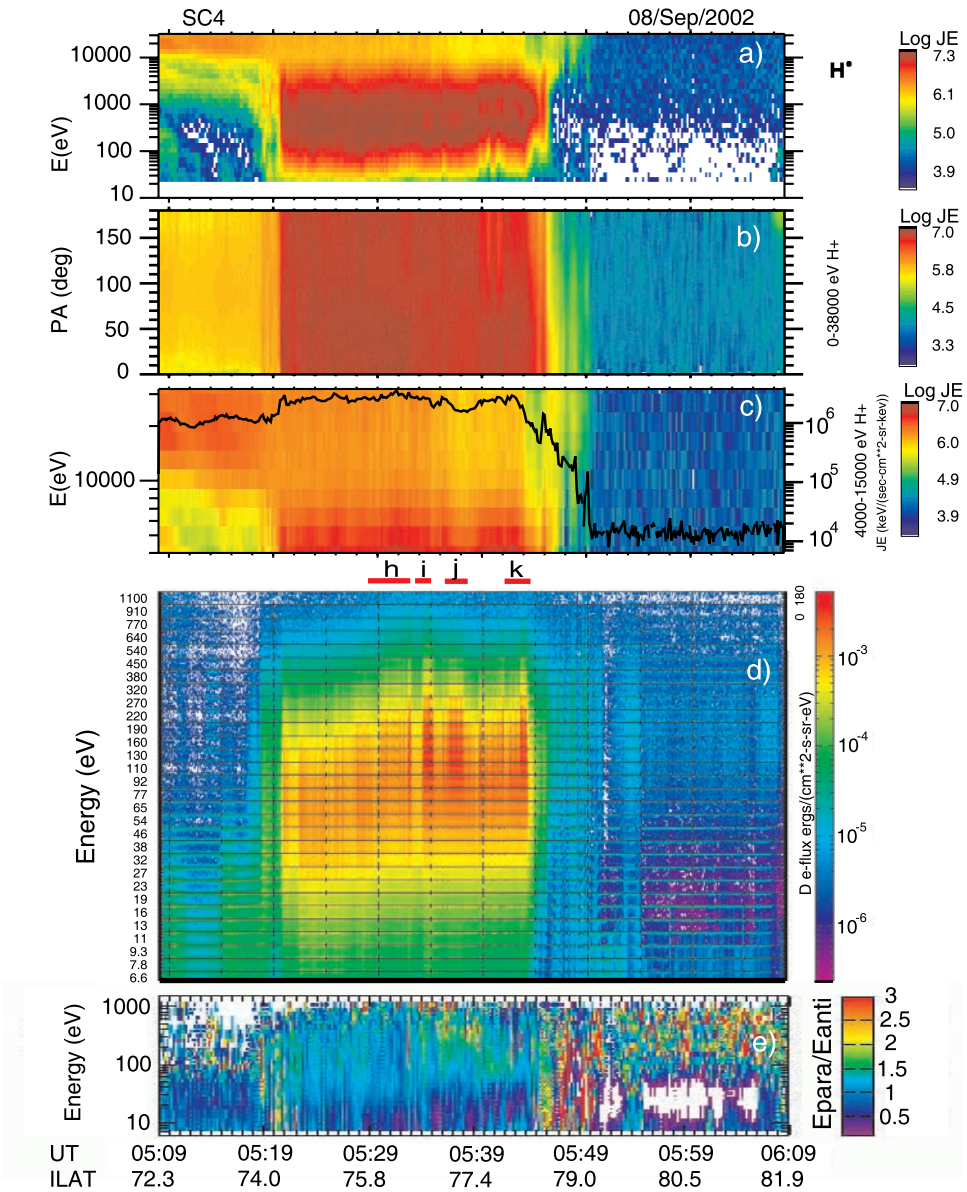

Figure 5. Electron and ion data based on the PEACE LEEA and CIS-CODIF observations on SC4 on 8 September 2002 from 0509 to 0609 UT. Same format as Figure 3. The short bold lines in the middle indicate times corresponding to the separate electron beams h–k discussed in the text.

spectrogram of H^+ ions, we observe reversed energy-time dispersion from ~0530 UT. The reverse low-energy cutoff is observed from ~0515 UT. It is also interesting to note that the ion population detected on SC4 is "broader" in comparison with the population observed on SC1. Thus, energies of magnetosheath-like H^+ ions detected on SC4 are E = 30–10000 eV (Figure 5a). High-energy ions (E = 4–15 keV) are detected generally throughout the cusp crossing, however it is possible to see some particular flux enhancements before 0535 UT (beams h and i) and 0536–0537 UT and 0539–0544 UT (beam k). The spikes of magnetosheath-like ion population with additional high fluxes at high energies correspond partially to the electron beams. Additionally, significant fluxes of ions with plasma sheet energies are detected during this cusp crossing, especially during the interval 0519–0535 UT. However, we should note that the CIS-CODIF instrument saturates in high-density plasma, and thus such strong ion fluxes observed on SC4, especially at high energies, can be partially due to saturation effects.

[26] From ~0521 UT to ~0539 UT, the parallel velocity is very low, V_{para} = ±20 km s^{-1} and the perpendicular velocity is less than 20 km s^{-1}, with convection being slightly sunward, V_{perp_x} = 0–10 km s^{-1}, and mostly dawnward, V_{perp_y} varies from 5 to −20 km s^{-1}. Thus, convection is much lower than that observed inside the cusp by SC1. We can consider this part of the cusp as being nearly stagnant. The ions inside the cusp are isotropic, which also indicates a nearly stagnant cusp. From ~0539 UT, the plasma injections are evident, with V_{para} = 50–200 km s^{-1}. The pitch angle spectrogram shows that the downgoing population slightly dominates. At this time, the plasma moves sunward, V_{perp_x} = 20–60 km s^{-1}, and dawnward, V_{perp_y} varies from 0 to −50 km s^{-1}. We

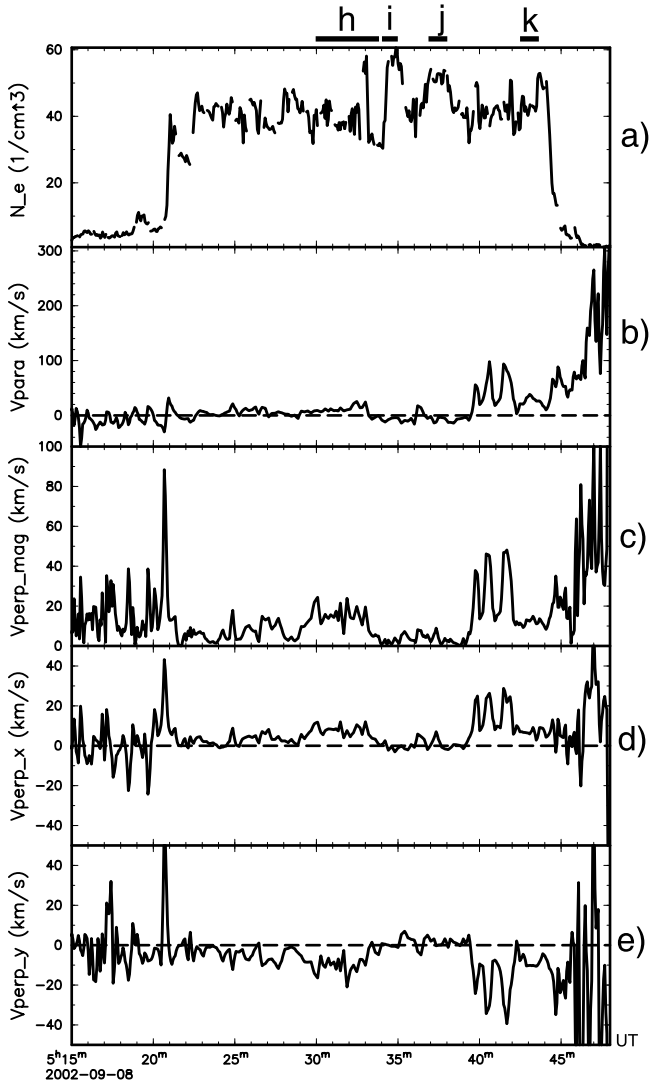

Figure 6. The plasma parameters calculated on the basis of the PEACE and CIS-CODIF observations on SC4 on 8 September 2002 from 0515 to 0548 UT. Same format as Figure 4. The short bold lines above the plot indicate times corresponding to the separate electron beams h–k discussed in the text.

observe ion injections at the poleward boundary of the cusp, which is again a signature of lobe reconnection.

[27] To summarize, SC4 crosses the cusp during the period when the IMF remains strongly northward. SC4 detects some plasma properties similar to the SC1 observations inside the cusp; especially, the bidirectional electron beams with similar parallel and antiparallel fluxes at all energies in the nearly stagnant cusp region are commonly observed. These beams are observed simultaneously with an increase of ion fluxes with energies 4 keV $< E <$ 10 keV. However, the convection inside the cusp observed by SC4 is lower than that observed by SC1.

3.4. Cusp Crossing Observations by Cluster 3

[28] An overview of the SC3 plasma data is shown in Figures 7 and 8 whose formats are again similar to Figures 3 and 4, respectively. Before ~0605 UT, SC3 is in the dayside plasma sheet, characterized by high-energy ion population (Figure 7a). From ~0604 UT SC3 begins to detect the magnetosheath-like ions with energy ranged from 80 to 400 eV about 64 min after SC1. From ~0605 UT, the population of magnetosheath-like ions is enhanced, and their energy band broadens to 20–2000 eV. During this period, the ion spectrogram shows low-energy cutoff decreasing with latitude. The peak of injection is detected from ~0605 to ~0606 UT. Then the fluxes reduce until ~0608 UT. From ~0608 UT, the ion fluxes are significantly enhanced and remain high until the end of the cusp crossing. From 0604 to ~0607 UT, the plasma sheet-like ions with energies between 8 and 38 keV are still seen (Figures 7a and 7b). Figure 8b shows a net parallel flow between ~0605 and 0607 UT with $V_{para} = 0–60$ km s^{-1}, which indicates plasma injections. The plasma convection defined by the perpendicular velocity is weak ($V_{perp} < 15$ km s^{-1}). The X component of the perpendicular velocity ranges between 0 and -2 km s^{-1} from 0604 to 0606 UT (which is zero in the error range), and it becomes variable between ±15 km s^{-1} from 0606 to 0610 UT (Figure 8c). The Y component of the perpendicular velocity changes its direction at about 0605 UT and reaches its maximum value of 15 km s^{-1} (Figure 8e). Before 0605 UT, dawnward convection dominates, while after 0605 UT, duskward convection dominates. As the convection velocity is very low, we may also refer this period as stagnation. The electron density presented in Figure 8a also shows a separate injection between 0605 and 0607 UT. A nearly bidirectional electron beam is detected at ~0606 UT (Figures 7d and 7e), with energy ranging from 25 to 260 eV. During the interval 0606–0608 UT, the reduced fluxes of the magnetosheath-like electrons are detected.

[29] From ~0608 UT, magnetosheath-like electrons with normal fluxes are continuously detected. Generally electrons inside this cusp crossing are not isotropic. The intensity of the electron fluxes is variable, mainly in the energy range 22–440 eV, and dominated by an upgoing (pitch angle ~180°) population (Figure 7d). For the energy range 20–41 eV, the electrons are also mainly upgoing. Figure 8a shows several peaks in the electron density, at 20–30 cm^{-3}, which indicates the multiple injections of electrons. We can identify these electron beams at ~0610 UT (beam l), 0611–0614 UT (beam m), 0616–0618 UT (beam n), 0618–0620 UT (beam o), 0621–0624 UT (beam p), 0625–0626 UT (beam q), and 0627–0629 UT (beam r). For all these beams, the upgoing population dominates in the energy band 14–310 eV (Figures 7d and 7e). However, beams o, p, and q are much more populated in the energy band around 280 eV and still populated in the energy band around 430 eV. Moreover, at the high-energy end (~280 eV), these beams are nearly bidirectional. The time periods of electron beams n, o, p, q, and r correlate very well with observed enhancements of the fluxes of the high-energy part of the magnetosheath-like population (Figure 7c).

[30] During the interval 0610 to 0625 UT, the ion parallel velocity is very low, $V_{para} = ±20$ km s^{-1}. The X component of the convection velocity remains less than 10 km s^{-1} and the Y component remains less than 15 km s^{-1}. Despite the low speed the convection keeps mainly sunward and duskward, consistent with the expectation of lobe reconnection under negative IMF B_Y. We refer to this region

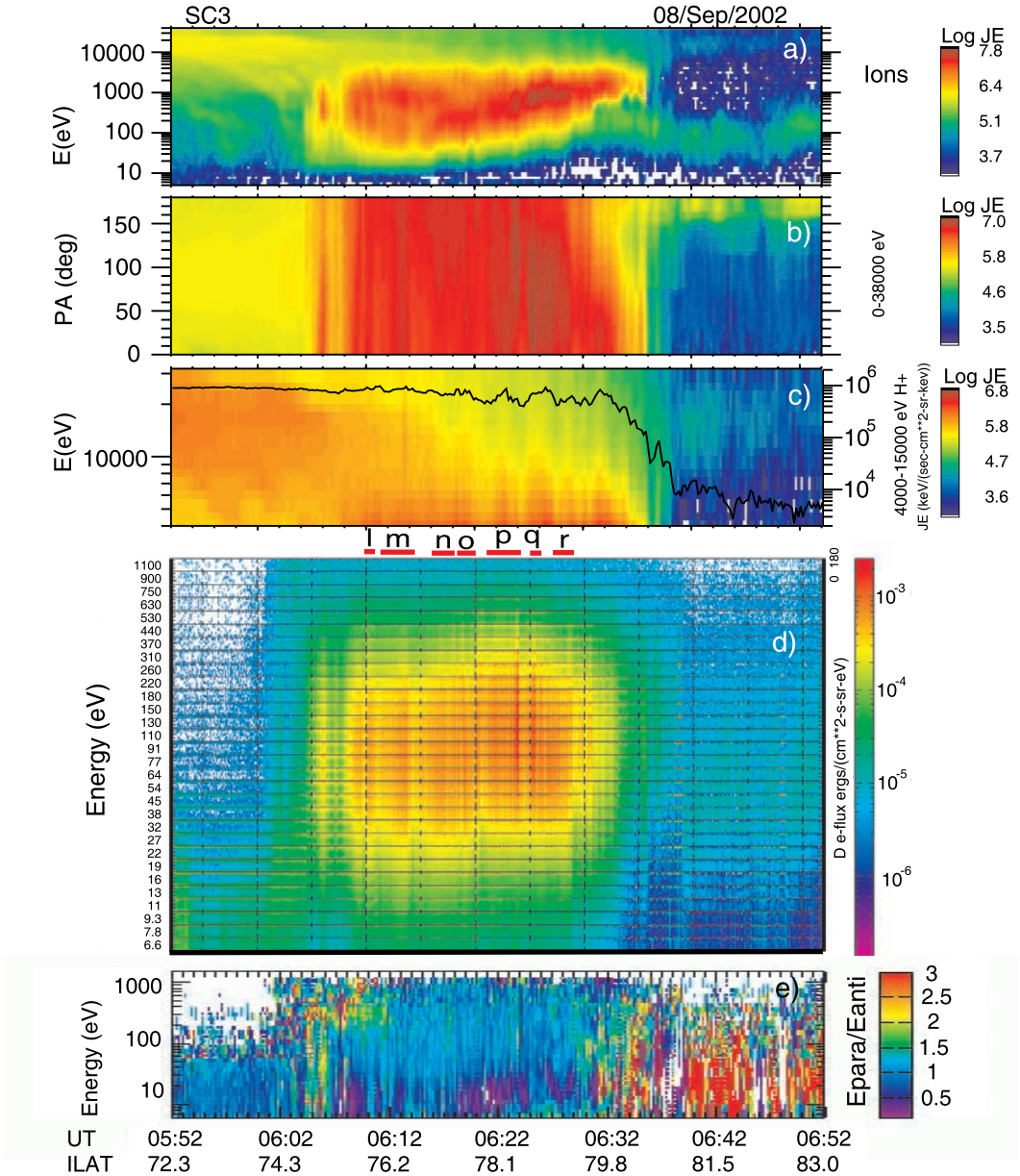

Figure 7. Electron and ion data based on the PEACE LEEA and CIS-HIA observations on SC3 on 8 September 2002 from 0552 to 0652 UT. Same format as Figure 3. The short bold lines in the middle indicate times corresponding to the separate electron beams l–r discussed in the text.

as the nearly stagnant cusp, because the convection velocity is much lower than that observed near the poleward boundary, where the X component of the convection velocity is $\sim$10–50 km s^{-1}.

[31] Between $\sim$0625 and 0640 UT, Cluster SC3 moves from the cusp into the northern lobe region, and crosses the poleward boundary of the midaltitude cusp at $\sim$0636 UT. This region is characterized by the appearance of strong downgoing magnetosheath-like ion injections (Figure 7b), high fluxes of short-duration electron beams (Figure 7d), net field-aligned flow, $V_{para} \sim$ 20–200 km s^{-1}, and strong sunward convection, V_{perp_x} = 10–50 km s^{-1} (Figures 8b and 8d). The ion spectrogram shows a clear low-energy cutoff at the poleward boundary of the cusp and reversed energy-time dispersion, which are again signatures of the lobe reconnection process [e.g., *Reiff et al.*, 1980; *Burch et al.*, 1980; *Smith and Lockwood*, 1996]. Plasma convection past the spacecraft is mainly sunward with the X component of the perpendicular velocity remaining positive and varying up to 50 km s^{-1}. The Y component of the perpendicular velocity is highly variable between 20 and $-$20 km s^{-1}. From 0636 UT, SC3 leaves the cusp and moves into the lobe region of the magnetosphere.

[32] To summarize, SC3 enters the cusp when the IMF has remained strongly northward (IMF clock angle $\sim$0–20°) for more than 1 h. SC3 detects a separate population on the cusp equatorward boundary, a nearly stagnant part in the middle, and the features of lobe injection near the poleward boundary. Electron beams in the nearly

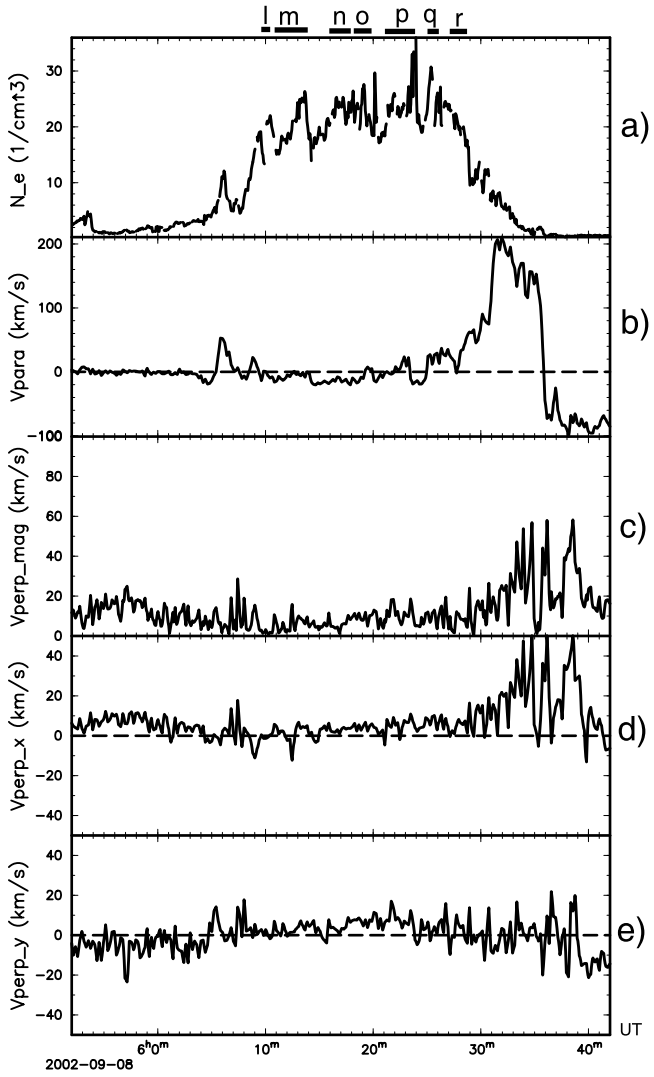

Figure 8. The plasma parameters calculated on the basis of the PEACE and CIS-HIA observations on SC3 on 8 September 2002 from 0550 to 0641 UT. Same format as Figure 4. The short bold lines above the plot indicate times corresponding to the separate electron beams l–r discussed in the text.

stagnant cusp region are also observed, but they are not completely bidirectional.

3.5. Azimuthal Cuts Through the Electron Energy Spectra and Ion Phase Space Density Distributions

[33] The above observations show that the Cluster satellites detect high-energy electron and ion fluxes for some periods during the cusp crossing. Some of the electron beams seem to be nearly bidirectional on the electron spectrogram. We examine the electron azimuthal cuts through the electron energy spectra and ion phase space density distributions, which may provide detailed information on the plasma characteristics observed by the three spacecraft. We look into electron azimuthal cuts of differential energy flux and ion distribution functions every 1 min during the cusp crossing. During the periods having the high-energy electron fluxes, and additionally accelerated ions, we examine electron energy spectra every 4 s (spin resolution) and the ion distribution functions every 20 s. These time selections are based on the assumption that the electrons maybe highly variable and the spectra may change significantly within 4 s. Contrary, the ions are heavier and thus the timescale can be larger.

[34] Some results of our study are shown in Figures 9, 10, and 11 which correspond to observations from SC1, SC4, and SC3, respectively. Figures 9, 10, and 11 all have a similar format and show electron azimuthal cuts through the electron energy spectra and H^+ phase space density distributions based on the PEACE LEEA and CIS-CODIF observations for the particular time intervals indicated above each column. The first row shows the electron 2-D azimuthal cuts of the electron spectra in the differential energy flux units, in which 0° (top) indicates the direction parallel to the local magnetic field, and 180° (bottom) indicates the direction antiparallel to the local magnetic field. The differential energy flux is color coded, and the same scale has been used for all columns. The second row shows the cross sections of the 2-D cuts in the parallel, perpendicular and antiparallel directions. The right half of the plot corresponds to particles flowing in the direction of the chosen cut angle, thus the black line corresponds to 0° pitch angle particles, the green line corresponds to 90° pitch angle particles and the red line corresponds to 180° particles. The left half of the plot corresponds to particles traveling in the opposite direction of the chosen cut angle. Thus, the legend is reversed for this part of the plot, i.e., the black line corresponds to 180° pitch angle particles, the green line corresponds to 90° pitch angle particles and the red line corresponds to 0° particles. The third row presents the 2-D cross sections of the H^+ ion distribution functions in a plane containing (V_{para}, V_{perp}). V_{para} is aligned with the local magnetic field, and V_{perp} is in the $-(V \times B) \times B$ direction. The colors represent the phase space density. Contours are evenly spaced logarithmically between the minimum and maximum values. The same scale has been used for all columns. $V_{para} > 0$ corresponds to the downgoing population and $V_{para} < 0$ corresponds to the upgoing population. The fourth row shows the 1-D cross sections of the H^+ ion distribution along the magnetic field direction ($V_{perp} = 0$, black line) and perpendicular to the magnetic field direction ($V_{para} = 0$, green line).

[35] In the SC1 observations we note that beams b and d have high-energy electrons and accelerated ions. We compare plasma properties during beams b and d with those during beams f and g near the cusp poleward boundary. Figure 9 shows three electron azimuthal cuts through the electron energy spectra and ion phase space density distributions from SC1: one example (~0520 UT) for beam b, one example (~0529 UT) for beam d, and one example (~0535 UT) for beam f. The 1-D cross sections of the electron 2-D cuts (second row) indicate that at ~0520 UT and ~0529 UT the fluxes of parallel and antiparallel populations are generally higher than the perpendicular populations for energies below 500 eV. Above 500 eV, the fluxes in the parallel, antiparallel and perpendicular directions are nearly equal. Additionally the parallel and antiparallel populations have very well balanced fluxes for energies above 40 eV. For the low-energy (10–40 eV) bin, the antiparallel electron flux exceeds the parallel one. Contrary, at ~0535 UT, near

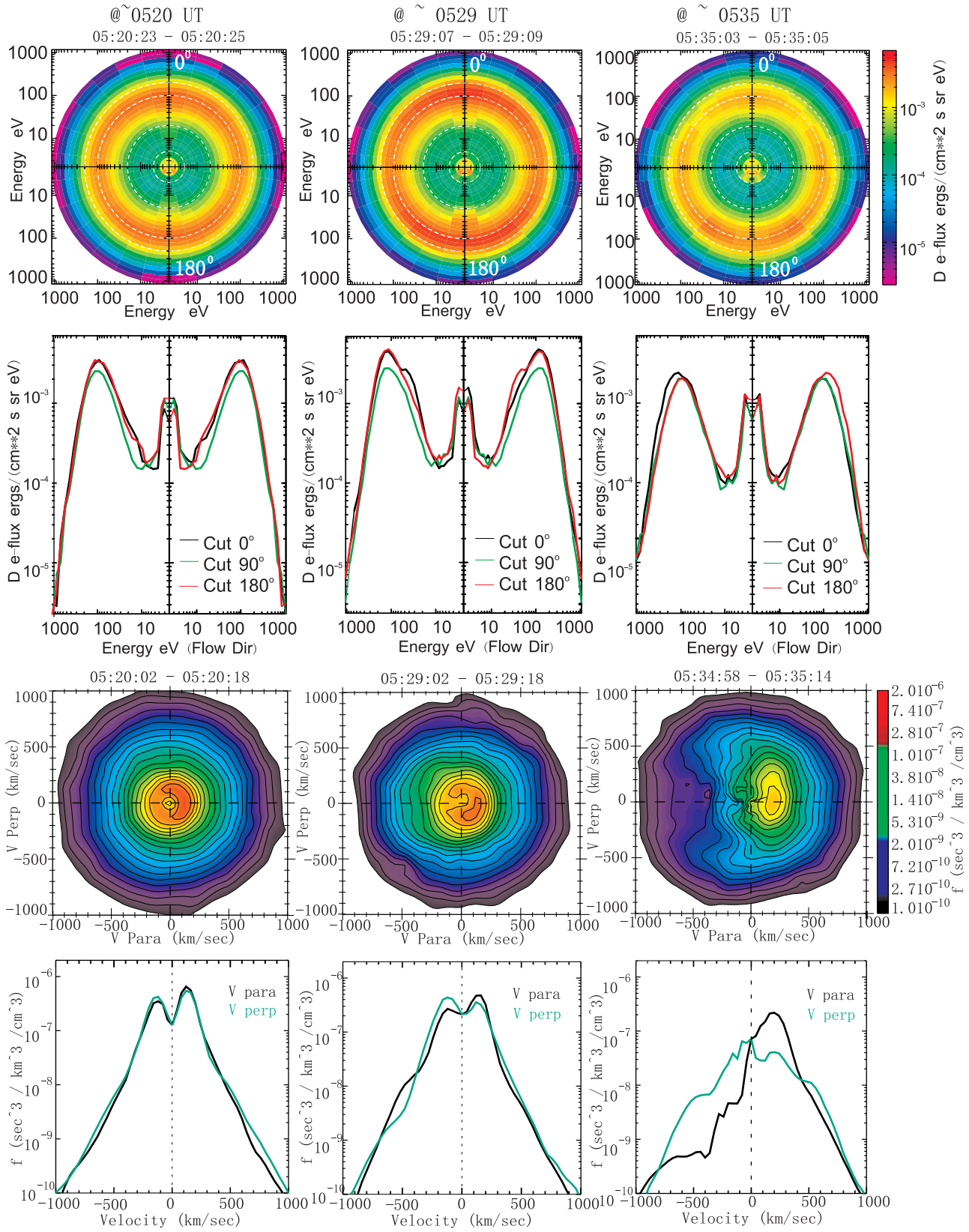
@~0520 UT
05:20:23 - 05:20:25
@ ~ 0529 UT
05:29:07 - 05:29:09
@ ~ 0535 UT
05:35:03 - 05:35:05
Energy eV
D e-flux ergs/(cm**2 s sr eV)
Cut 0°
Cut 90°
Cut 180°
Energy eV (Flow Dir)
05:20:02 - 05:20:18
05:29:02 - 05:29:18
05:34:58 - 05:35:14
V Perp (km/sec)
V Para (km/sec)
f (sec^3 / km^3 /cm^3)
V para
V perp
Velocity (km/sec)

Figure 9

the poleward boundary of the cusp, the upgoing electron population with energies above ~100 eV is dominant, and counterstreaming populations are not balanced. Above 500 eV, the fluxes of the perpendicular population are nearly equal to the fluxes of parallel and antiparallel populations. In the ion distributions, at ~0520 and ~0529 UT, along the presumably reclosed field lines, we observe nearly isotropic ion distribution, with some enhancement of downgoing fluxes. At the same moments, the parallel and perpendicular 1-D cuts of the ion population are similar, also indicating that ions are quasi-isotropic. At ~0535 UT, near the poleward boundary we observe a D-shaped ion distribution. The downgoing ion population clearly dominates, which indicates the ongoing plasma injections at this time. Comparison of 1-D cuts of the ion population at this time shows that the perpendicular velocity is higher than the bulk parallel velocity of the upgoing population.

[36] Similar observations are presented for SC4 in Figure 10. Beams h, i, and j have high-energy electrons and accelerated ions. We show three examples (~0531 UT (inside beam h), ~0535 UT (inside beam i), and ~0538 UT (inside beam j)) for these beams, as well as one example (~0544 UT) near the poleward boundary of the cusp. As one can see, inside beam h, fluxes of counterstreaming electrons are very well balanced at nearly all energies. Inside beams i and j fluxes of counterstreaming electrons are balanced for higher energies, above ~100 eV. For the population with energies ~100 eV (near mean energy), there are some small disagreements between fluxes of downgoing and upgoing populations. This disagreement gets larger for energies less than 40 eV. Thus, it is possible to conclude that for beams i and j the electron population is bidirectional with nearly equal fluxes at energies above 40 eV. Near the poleward boundary (Figure 10 fourth column), we observe dominant parallel population at energies above 70 eV and dominant antiparallel population at energies below 70 eV. Thus, this population is strongly unbalanced. We also should note that the electron spectra are very variable throughout the cusp and small changes are seen every spin. Thus, the ideal situation when the counterstreaming electron population is completely balanced at all energies is rarely seen. The presented electron spectra during beams i and j are more typical, when there is a good balance for the high-energy electron population, $E > 100$ eV, and there are some small disagreements between bidirectional fluxes at ~70–110 eV. In the ion distributions, we observe, similar to the SC1 case, nearly isotropic ions inside beams h, i, and j, along the presumably reclosed field lines. Near the poleward boundary of the cusp, more anisotropic ion population is seen.

[37] We analyze electron and ion data in the same way for SC3. Beams o, p, and q have high-energy electrons and accelerated ions. In Figure 11, we show four examples for each beam o (~0619 UT), p (~0623 UT), q (~0625 UT), and r (~0627 UT), as well as one example (~0631 UT) near the poleward boundary of the cusp. From the electron pitch angle spectrogram (Figure 7d) it is clear that at lower energies, upgoing electrons dominate. Domination of the upgoing electrons at low energies is also evident from the presented electron spectra. Thus, fluxes of the counterstreaming electrons are unbalanced at energies 20–200 eV. However, for the examples during beams o, p, and q we observe the bidirectional properties at high energies, above ~200 eV. For these events the fluxes of parallel and antiparallel populations with energies above 200 eV are nearly equal. For the example near the poleward boundary, we observe the dominant parallel injections at some energies, $E \sim 200$–900 eV. The similar domination of downgoing electrons with energies 200–1000 eV is observed at 0628 UT, inside beam r. The ion distribution functions detected on SC3 are significantly different to those observed by SC1 and SC4. Indeed, we do not observe isotropic distributions in this case. Along the presumably reclosed field lines, when the electron counterstreaming population has nearly equal fluxes in the parallel and antiparallel directions for high-energy part of population, the ion distributions are D-shaped and show clear positive and negative low-velocity cutoffs.

3.6. Ion Distribution Near the Equatorward Boundary Observed on SC3

[38] To investigate this anisotropic ion population observed on SC3 further, we study the ion distribution

Figure 9. Electron azimuthal cuts through the electron energy spectra and H^+ phase space density distributions based on the PEACE LEEA and CIS-CODIF observations on SC1 on 8 September 2002 at ~0520 (beam b), ~0529 (beam d), and ~0535 UT (near the cusp poleward boundary). The first row shows the electron 2-D azimuthal cuts of the electron spectra in the differential energy flux units, in which 0° indicates direction parallel to the local magnetic field (top) and 180° indicates direction antiparallel to the local magnetic field (bottom). The differential energy flux is color coded, and the same scale has been used for all three plots. The second row shows the cross sections of the 2-D cuts in the parallel, perpendicular, and antiparallel directions. The right half of the plot corresponds to particles flowing in the direction of the chosen cut angle, thus the black line corresponds to 0° pitch angle particles, the green line corresponds to 90° pitch angle particles, and the red line corresponds to 180° particles. The left half of the plot corresponds to particles traveling in a direction (180°-cut angle). Thus, the legend is reversed for this part of the plot, i.e., the black line corresponds to 180° pitch angle particles, the green line corresponds to 90° pitch angle particles, and the red line corresponds to 0° particles. The third row presents the 2-D cross sections of the H^+ ion distribution functions in a plane containing (V_{para}, V_{perp}). V_{para} is aligned with the local magnetic field, and V_{perp} is in the $-(V \times B) \times B$ direction. The colors represent the phase space density. Contours are evenly spaced logarithmically between the minimum and maximum values. The same scale has been used for all columns. The fourth row shows the 1-D cross sections of the H^+ ion distribution along the magnetic field direction ($V_{perp} = 0$, black line) and perpendicular to the magnetic field direction ($V_{para} = 0$, green line). Electron data used for these plots are accumulated over one spin around the time of interest, indicated above the plot, and ion data are accumulated over three to four spins to improve accuracy.

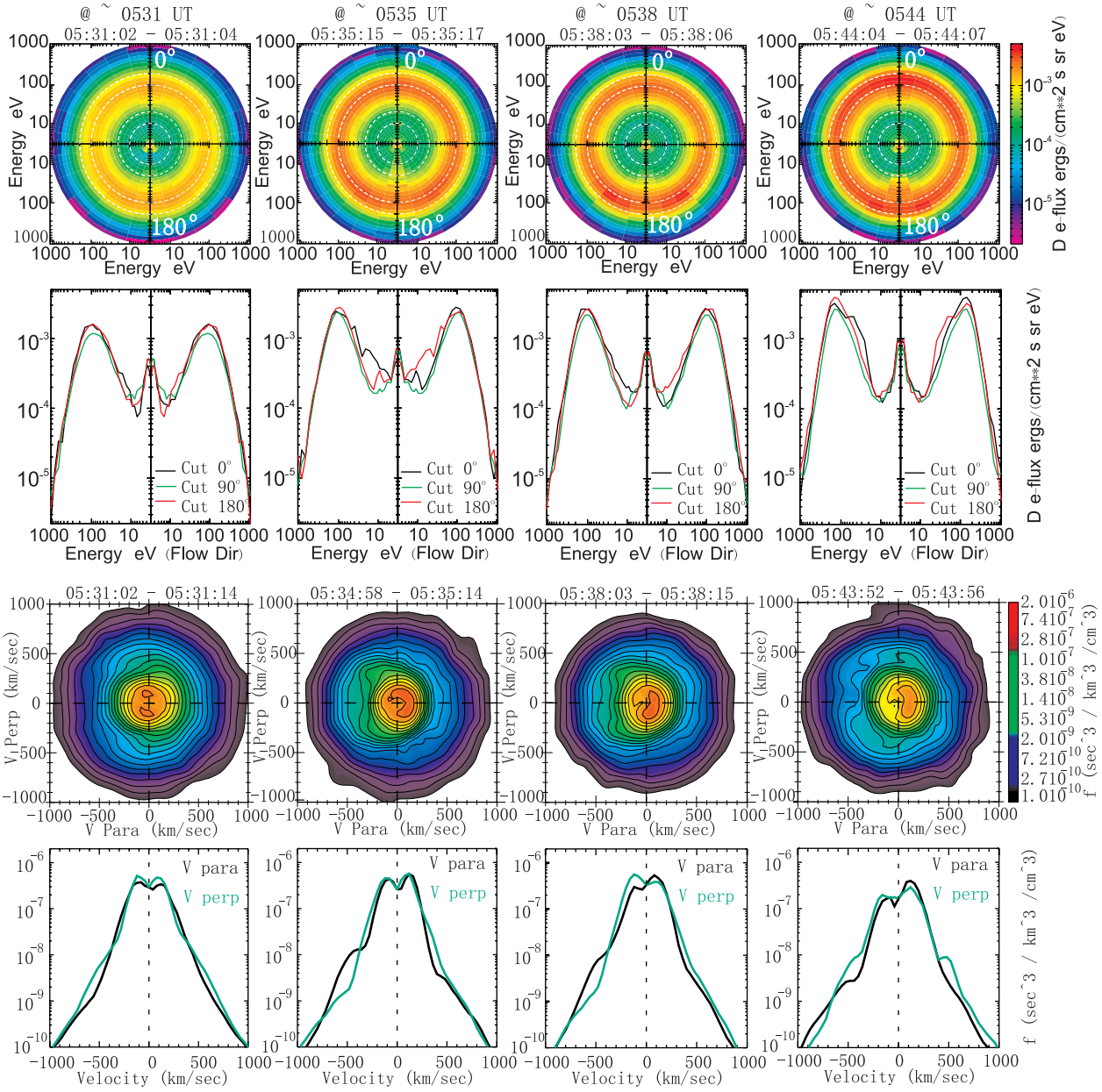

Figure 10. The azimuthal cut through the electron energy spectra and H^+ phase space density distributions based on the PEACE LEEA and CIS-CODIF observations on SC4 on 8 September 2002 at ~0531 UT (beam h), ~0535 UT (beam i), ~0538 UT (beam j), and ~0544 UT (near the cusp poleward boundary). Same format as Figure 9.

functions near the equatorward boundary of the cusp in more detail. We examine the ion distributions every 4 s (the basic time resolution) between 0604 and 0608 UT. We find two subintervals with different ion properties. Examples of these subintervals are illustrated in Figure 12. Each column shows a 4 s ion velocity distribution at one of the subintervals and the time interval is indicated on the top of the column. The first row shows the 2-D cuts of the ion distribution function parallel and perpendicular to the local magnetic field. The phase space density is color coded. The second row shows the 1-D cross sections of the H^+ ion distribution at $V_{perp} = 0$ (black line) and $V_{para} = 0$ (green line).

[39] From 0604 to 0605 UT (Figure 12 left), the distributions have mainly three characteristics: a lack of a mirrored ion population (there is no D-shaped population for the negative parallel velocity); a high-energy downgoing population and two positive low-velocity cutoffs. Thus this period is dominated by the downgoing injections. However, it seems that there are two parts in the positive D-shaped downgoing population. The low-energy population is D shaped, whose V_{para} and V_{perp} are below 200 km s^{-1}, while the high-energy population for $V_{para} > 400$ and $V_{perp} > 400$ km s^{-1}, which is clear and separated, shows again typical D shaped and implies injection of ions with very high energy. From the cross section at $V_{perp} = 0$, several positive parallel velocity cutoffs can be identified (in the downgoing population). The first cutoff is about 80 km s^{-1}, and the second is about 200 km s^{-1}. Sometimes a third cutoff can also be

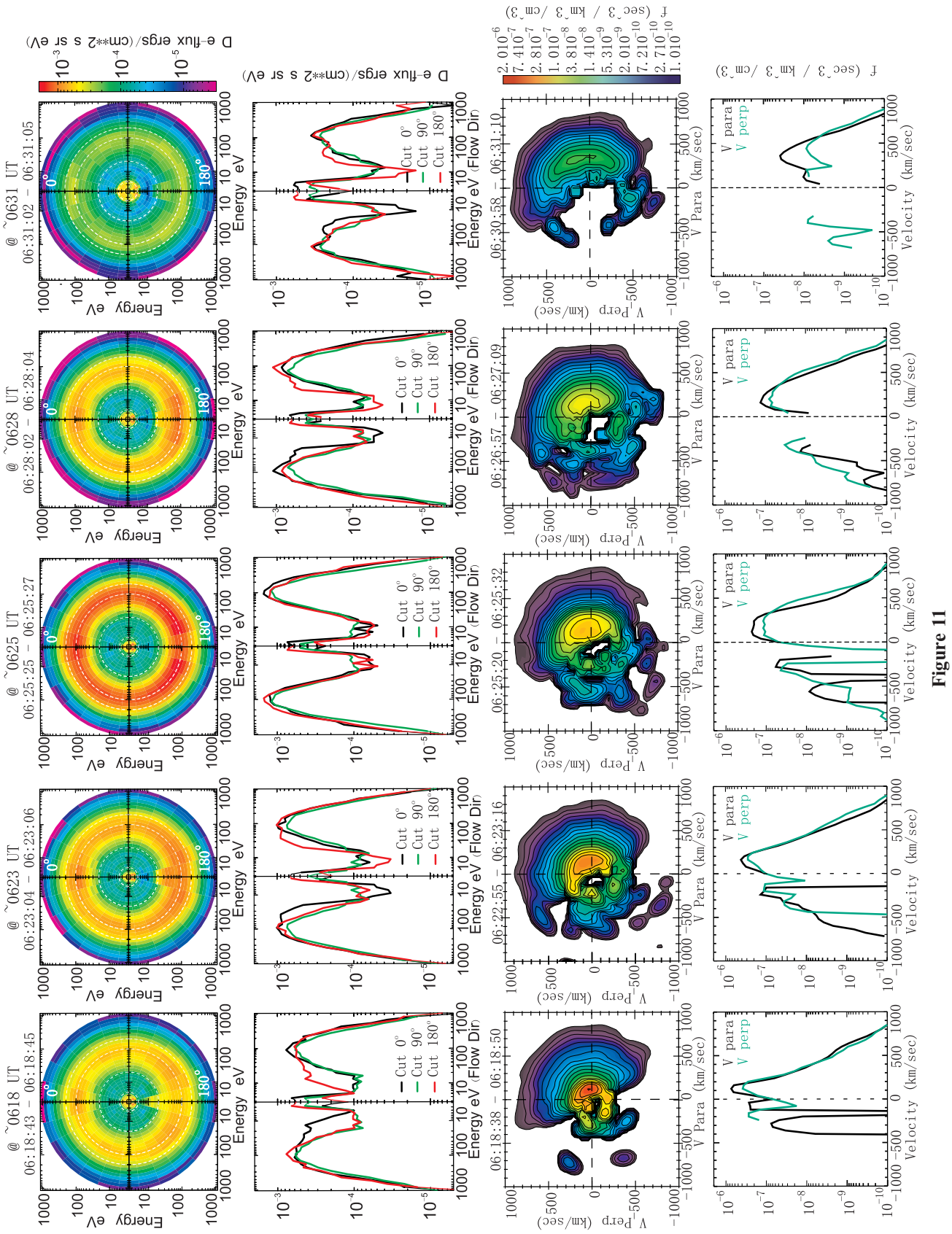
@ ~0618 UT
06:18:43 - 06:18:45
@ ~0623 UT
06:23:04 - 06:23:06
@ ~0625 UT
06:25:25 - 06:25:27
@ ~0628 UT
06:28:02 - 06:28:04
@ ~0631 UT
06:31:02 - 06:31:05
Energy eV
Energy eV (Flow Dir)
Cut 0°
Cut 90°
Cut 180°
D e-flux ergs/(cm**2 s sr eV)
06:18:38 - 06:18:50
06:22:55 - 06:23:16
06:25:20 - 06:25:32
06:26:57 - 06:27:09
06:30:58 - 06:31:10
V_Perp (km/sec)
V Para (km/sec)
V para
V perp
Velocity (km/sec)
f (sec^3 / km^3 /cm^3)

Figure 11

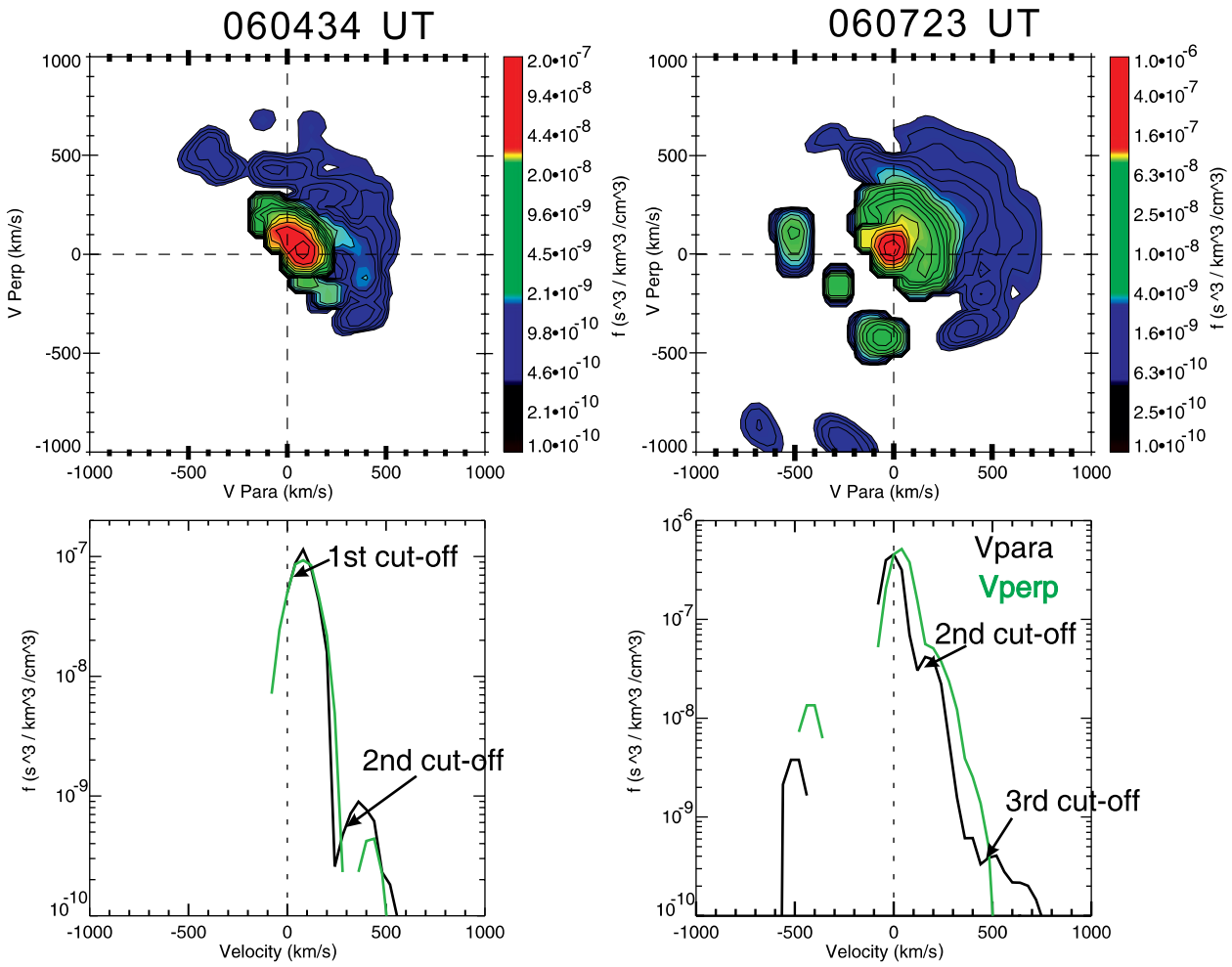

Figure 12. Examples of H^+ phase space density distribution based on the observations of CIS-CODIF instrument on the Cluster-SC3 for the 0604–0605 UT time interval and the 0605–0608 UT time interval. The first row shows the 2-D cuts through the ion distribution. The phase space density is color coded. The second row presents the 1-D cross sections of the H^+ ions phase space density in the parallel to the magnetic field direction, $V_{perp} = 0$ (black line), and in the perpendicular direction, $V_{para} = 0$ (green line).

seen (300–400 km s^{-1}). Each low-velocity cutoff might indicate an independent injection, so there are several independent injections in this period on the same field line.

[40] In the second subinterval, from ~0605 UT, the mirror ion population appears, as shown in Figure 12 (right). The negative low-velocity cutoff appearing in this period is between 400 and 600 km s^{-1}. The high-energy population mixes with the low-energy population and forms one D-shaped population in the downgoing particles. The second and third velocity cutoffs gradually decrease, until ~0608 UT, when they could not be discerned in the cross sections anymore.

[41] In summary, ion distributions observed by SC3 show the following special features (Figures 11 and 12):

[42] 1. Dominant downgoing ions. Two distinct D-shaped distributions are observed near the equatorward boundary of the cusp and one D-shaped distribution is commonly observed through the rest of the cusp.

[43] 2. Several upgoing ion populations near the equatorward boundary. There are usually two mirrored populations, and two low-velocity cutoffs on the cross section at $V_{perp} = 0$. These features require further investigation.

[44] 3. On the cusp poleward boundary, we observe the usual lobe reconnection precipitating features.

4. Interpretation and Discussion

4.1. Four Spacecraft Comparison and Cusp Size Variations

[45] Now we compare the observations by the four Cluster spacecraft. For the SC2 observations, we use data from the PEACE experiment only. Because of high

Figure 11. The azimuthal cuts through the electron energy spectra (differential energy flux is color coded) and H^+ distribution functions (phase space density is color coded) based on the PEACE LEEA and CIS-CODIF observations on SC3 on 8 September 2002 at ~0618 UT (beam o), ~0623 UT (beam p), ~0625 UT (beam q), ~0628 UT (beam r), and ~0631 UT (near the cusp poleward boundary). Same format as Figure 9.

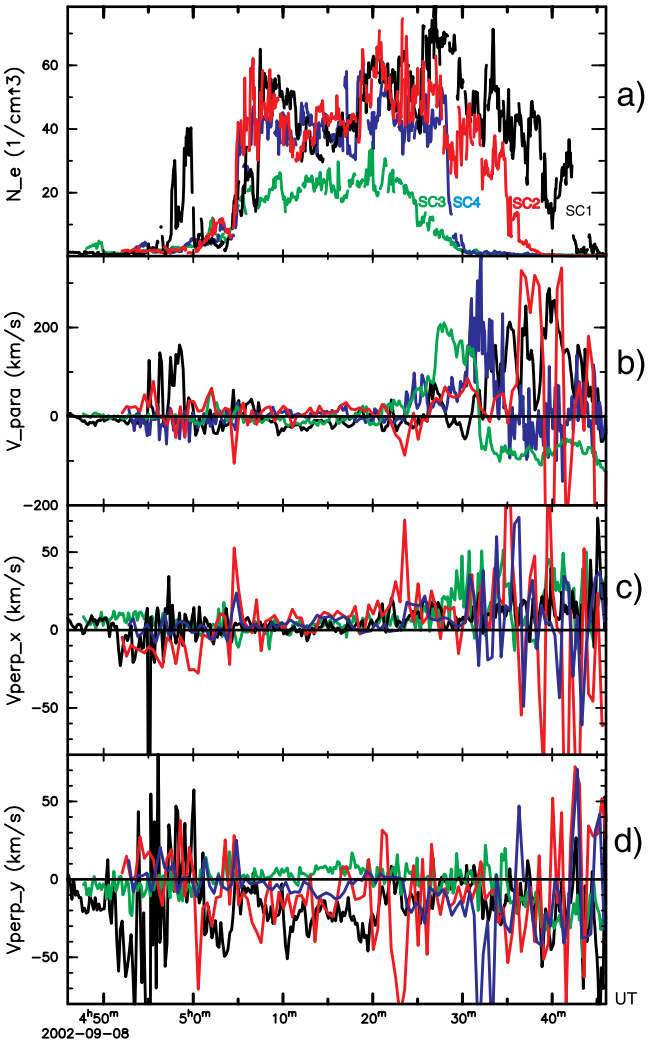

Figure 13. The plasma parameters calculated on the basis of the PEACE and CIS observations on four Cluster satellites on 8 September 2002. (a) The electron density and (b–d) the ion bulk velocity in the magnetic field-aligned coordinate system: the parallel velocity (Figure 13b), and the X and Y components of the perpendicular velocity (Figures 13c and 13d, respectively). The GSM coordinate system has been used for the velocity components. For the density estimation the electron data have been used from all four spacecraft. For the velocity estimation the CIS-HIA observations have been used from SC1 and SC3, the CIS-CODIF observations from SC4 (averaged over 30 s), and the PEACE observations from SC2 (averaged over 30 s). The Cluster color code has been used: SC1 is black, SC2 is red, SC3 is green, and SC4 is blue. For better comparison the time series of SC2 are shifted backward by 5 min, the time series of SC4 are shifted backward by 16 min, and the time series of SC3 are shifted backward by 64 min.

telemetry rate on SC2, we can calculate plasma parameters (density and velocity) using 3-D data available with high time resolution. Figure 13 presents a combined plot of the plasma parameters calculated on the basis of the PEACE and CIS observations on four Cluster satellites on 8 September 2002. Figure 13a presents the electron density with 4 s resolution and Figures 13b–13d show the ion bulk velocity in the magnetic field-aligned coordinate system: the parallel velocity (b), and the X and Y components of the perpendicular velocity (Figures 13c and 13d, respectively). The GSM coordinate system has been used for the velocity components. For the density estimation the electron data have been used from all four spacecraft. For the velocity estimation the CIS-HIA observations have been used from SC1 and SC3, the CIS-CODIF observations from SC4 (averaged over 30 s), and the PEACE observations from SC2 (averaged over 30 s). The Cluster color code has been used: SC1 is black, SC2 is red, SC3 is green, and SC4 is blue. For better comparison, the time series of SC2 are shifted backward by 5 min, the time series of SC4 are shifted backward by 16 min, and the time series of SC3 are shifted backward by 64 min. The time shifts are calculated from the comparison of the times of the crossings of the equatorward boundary of the cusp by the different spacecraft.

[46] We observe clearly different density levels during the four cusp crossing events. We cross checked the electron density from the PEACE instrument with the ion density from the CIS-HIA instrument, and we also cross checked the different PEACE products (3DR, SPINPAD and onboard). All densities agree with each other very well, hence the significance difference in the plasma density between the cusp crossings is not due to calibration errors. SC1 detects the densest plasma; the maximum density observed on SC1 is $\sim$80 cm^{-3}. Plasma density variations observed on SC2 are very similar to those on SC1, especially during the first 15 min of the cusp crossing. Having in mind that these two satellites are very close to each other, with a time difference of 5 min, we suggest that SC1 and SC2 cross the same plasma population, at least at the beginning of the cusp crossing. However, one special feature observed by SC1 is a separate density peak near the equatorward boundary of the cusp which corresponds to the separate population observed in the electron and ion spectrograms. Comparison of the densities suggests some similarity of the cusp structures during the SC1, SC2, and SC4 crossings. These spacecraft see a sudden outset of the dense plasma; the density tends to maintain the same level in the middle of the cusp; and the density increases significantly in several intervals near the poleward boundary of the cusp. However, SC4 observes a less dense plasma than previous two satellites and variations in the density are not very well related to variations observed by SC1 and SC2. The durations of the injections near the poleward boundary are different: SC1 observes these over a period of 15 min, SC2 for 10 min, SC4 for 7 min, and SC3 for 10 min.

[47] The most dramatic difference in the plasma density is detected on SC3. Indeed, the plasma density inside the cusp appears to decrease during the period of interest by a factor of $\sim$3 (from $\sim$60 to $\sim$20 cm^{-3}). This phenomenon is correlated to the density variation of the solar wind. From $\sim$0520 to $\sim$0640 UT, the solar wind density decreases by 38% (Figure 2e). The decrease of the plasma density inside the cusp is also correlated with the IMF being northward for more than 1 h. The statistical study of the cusp density agrees with our observations: it was shown that the cusp density is lower under northward IMF than under southward IMF (F. Pitout, private communication, 2007). We suggest

Table 1. Summary of the Positions of the Four Cluster Spacecraft When They Enter and Leave the Cusp[a]

	Enter (UT)	ILAT (degrees)	MLT	Leave (UT)	ILAT (degrees)	MLT	Cusp Crossing Duration (min)	Cusp Size (degrees)
SC1	0456	71.2	1151	0544	78.5	1209	48	7.3
SC2	0506	71.7	1203	0545	78.4	1232	39	6.7
SC4	0519	72.5	1157	0546	77.9	1211	27	5.4
SC3	0602	74.3	1214	0635	80.3	1246	33	6

[a]The positions are measured in (ILAT, MLT), and the cusp crossing duration is measured in minutes. The last column shows the cusp size indicated by the difference of the ILAT between the equatorward and poleward boundaries of the cusp.

that the difference in the density may not only be due to the solar wind effect, but may also be the result of a different effectiveness of reconnection processes during southward and northward IMF conditions. The other possible explanation can be that during this time interval the cusp moves in the longitudinal direction and SC3 crosses different part of the cusp, probably toward the edge. However, the IMF B_Y component, which is responsible for the cusp longitudinal motion [e.g., *Zhou et al.*, 2000], is relatively stable at ~+2 nT. Thus, we would not expect significant cusp motion in the longitudinal direction during this interval.

[48] The plasma parallel velocities observed on the four spacecraft show similar behavior: the parallel velocity is very low, ±20 km s^{-1}, near the equatorward boundary and inside the center of the cusp, and it becomes strong and positive toward the poleward boundary of the cusp, reaching 200–300 km s^{-1}. We also observe some interesting features from the comparison of the convection speeds. During each cusp crossing, we observe a region of very low sunward convection, which we identify as the ''nearly stagnant cusp'' or ''part of the cusp with reduced convection.'' Although the cusp crossing durations are conspicuously different, the duration of the nearly stagnant cusp crossing is always about 15 min. We note that inside the nearly stagnant cusp, the density variation from SC1 to SC3 is lower (from 40 to 20 cm^{-3}), and consistent with solar wind density variations. That suggests the nearly stagnant cusp is one stable region which is less affected by the convection near the boundaries of the cusp. We also note that inside the nearly stagnant cusp (or cusp region with reduced convection), SC1, SC2, and SC4 detect a mainly dawnward convection ($V_{perp\_y} \sim -(10–40)$ km s^{-1}), while SC3 detects a mainly duskward convection ($V_{perp\_y} \sim$ 10 km s^{-1}). However, the B_Y component of the IMF is duskward for all the three events. This suggests that the cusp observed by SC3 may have a different source. Such disagreement in the densities and velocities observed by three spacecraft, SC1, SC2 and SC4, and by SC3 reveals that SC3 crosses into newly formed cusp region, and despite of low convection inside the cusp region, it is still dynamic region and plasma properties inside the cusp changes in the timescale of 1 h, even under strong northward IMF. We also note that SC2 and SC4 detect a spike of positive convection near the equatorward boundary of the cusp, while SC3 detects a spike of antisunward convection. However, this happens when the satellites cross a region with a strong density gradient and thus such a strong velocity might be due to calculation errors.

[49] Thanks to the multispacecraft facilities provided by Cluster, we are able to estimate the motion of the cusp boundaries and the size of the cusp based on the four spacecraft observations. On the basis of the electron spectrograms, we determine the equatorward boundary of the cusp as a boundary when first magnetosheath electrons are observed. The poleward boundary of the cusp is determined from the electron densities when the density becomes comparable with the density inside the polar cap. We report the times and positions (magnetic local time (MLT), invariant latitude (ILAT)) where the spacecraft enter and leave the cusp in Table 1. From the boundaries of the cusp, we estimate the size of the cusp in ILAT at the time of each cusp crossing. We are aware that this estimation is not perfect, as the cusp might move during the time the spacecraft crosses it. However, the multispacecraft observations capacity of the Cluster provides us the possibility to observe directly the cusp motion and the cusp size variation. As seen from Table 1, the cusp shrinks from 7.3 to 5.4° ILAT between the SC1 crossing and SC4 crossing, and it expands to 6° ILAT between the SC4 crossing and SC3 crossing. One can see that the equatorward boundary of the cusp is constantly moving poleward, as observed by recurrent satellites. We estimate that the equatorward boundary generally moves toward high latitudes at the speed of 2.8° ILAT per hour, and it moves at the speed of 2.5° ILAT per hour between observations by SC4 and SC3. However, we do not observe constant motion of the poleward boundary of the cusp. Thus, the poleward boundary moves slightly poleward between observations by SC1 and SC2, it moves equatorward between observations by SC2 and SC4, and it moves poleward between observations by SC4 and SC3 with a speed of 2.9° ILAT per hour. It is interesting to note that while SC1, SC2, and SC4 enter the cusp at different times, they leave the cusp almost simultaneously.

[50] In summary, we note that in general the cusp moves antisunward, as defined from the motion of the equatorward boundary. At the beginning of the time of interest, when the cusp is crossed by SC1, SC2, and SC4, the cusp is shrinking, and the poleward boundary moves equatorward. Later, during the time interval between observations by SC4 and SC3, the poleward boundary moves poleward and the speed of the poleward boundary (2.9° ILAT per hour) is larger than that of the equatorward boundary (2.5° ILAT per hour), therefore the size of cusp expands at the speed of 0.4° ILAT per hour.

[51] There are a number of changes in the IMF and solar wind conditions during this event which might affect the motion of the cusp and cusp properties. Thus, the solar wind pressure pulse occurs at ~0607 UT, when SC1 enters the cusp. Similarly, the IMF changes orientation from southward to northward at the same time. The long period of stable northward IMF follows this change and during the rest of time interval the IMF configuration is favorable for the single or dual lobe reconnection.

[52] The antisunward movement of the cusp equatorward boundary can be explained by the sudden enhancement of

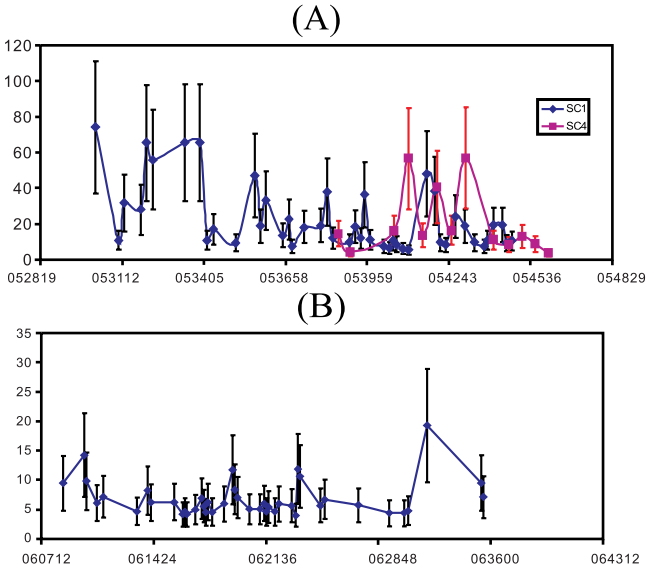

Figure 14. The distances from the (a) SC1 and SC4 and (b) SC3 to the reconnection site (X line) as a function of time based on the estimation of the low-energy cutoffs of the downgoing and mirroring ion populations. The distances are measured in R_E. The error bars show the uncertainty of 50%.

the solar wind dynamic pressure at ~0500 UT, which can possibly drive the whole cusp antisunward. Thus, Hawkeye observations showed that the cusp moves antisunward for higher values of solar wind dynamic pressure, if the Earth's dipole tilts away from the Sun [*Eastman et al.*, 2000]. However, this contradicts observations by *Newell and Meng* [1994] that the cusp moves equatorward when the solar wind pressure increases. Another possible explanation of this motion is the reaction of the cusp on the IMF northward turning, as illustrated in the case study by *Pitout et al.* [2006] and in the statistical study by *Newell et al.* [2006]. In this case, the reconnection site can move from the dayside magnetosphere to a location poleward of the cusp.

[53] In a single lobe reconnection event, the cusp size should not vary, because the footprints of the field lines circulate within the polar cap [e.g., *Cowley*, 1983; *Sandholt et al.*, 2000]. The significant expansion of the cusp size from the SC4 crossing to SC3 crossing suggests that other physical processes are going on. It was suggested that the dual lobe reconnection process will increase the cusp size, as it will create newly closed flux tubes inside the cusp region, and these flux tubes will be relatively stable [*Sandholt et al.*, 2000]. Thus, the net result of the secondary reconnection is the accumulation of field lines with the plasma precipitations, and an apparent expansion of the cusp size. Thus the expansion of the cusp size observed by SC4 and SC3 suggests the occurrence of the secondary reconnection, i.e., reconnection in the Southern Hemisphere lobe sector which recloses field lines previously reconnected in the lobe sector of the Northern Hemisphere. On the other hand, the decrease of the cusp size from SC1 to SC4 may result from the transitional phase of the IMF conditions. The outset of lobe reconnection may occur soon after the change in IMF orientation [e.g., *Pitout et al.*, 2006]. On the equatorward boundary, any residue open field lines created by earlier dayside reconnection exert antisunward pressure, while on the poleward boundary, lobe reconnection generates sunward movement. Thus, the net result of the establishment of the lobe reconnection might be a significant shrink of the cusp size.

4.2. Estimates of the Distance to the *X* Line

[54] As we observed plasma injections near the poleward boundary of the cusp on every Cluster spacecraft, we conclude that the northern lobe reconnection lasts for more than 100 min in our event. This is in agreement with previous IMAGE observations of the proton aurora inside the cusp region under northward IMF, showing that lobe reconnection may last for a few hours under stable conditions [e.g., *Frey et al.*, 2002]. And the three spacecraft observations provide us with the opportunity to study the movement of the reconnection site for a long term. The estimation of the distance from the spacecraft to the reconnection site is important, as it would help us in the determination of the location of the reconnection at the magnetopause and in the understanding of the reconnection geometry. Several methods to estimate the distance have been suggested [e.g., *Vontrat-Reberac et al.*, 2003]. Using the ion distribution functions, it is possible to estimate the distance to the reconnection line by using the low-velocity cutoffs of the precipitating and mirrored magnetosheath populations combined with a time of flight model and a semiempirical T96 magnetospheric model [e.g., *Trattner et al.*, 2004]. Since there are clear injections near the poleward boundary, we can apply this method. The distance, X, to the reconnection site is defined as

$$X/X_m = 2V/(V_m - V), \tag{1}$$

where X_m is the distance to the ionospheric mirror point, V is the cutoff velocity of the precipitating ions, and V_m is the cutoff velocity of the mirrored ions. X_m is determined by tracing the geomagnetic field line from the position of the spacecraft to the ionosphere by the T96 model [*Tsyganenko*, 1995]. In practice, the low-velocity cutoff of the distribution is defined at the lower speed side of each population where the flux is *1/e* of the peak flux [e.g., *Trattner et al.*, 2002, 2006]. The uncertainties in this method are significant, with an error in distance X of up to 50%, which mainly comes from the uncertainty of determining the low-velocity cutoffs of the mirrored distribution. Actually, the precipitating and mirrored populations do not present perfect low-velocity cutoffs and contain a lot of locally trapped ions [*Vontrat-Reberac et al.*, 2003]. Thus, this method should be applied for a sequence of observations and only the average result is likely to be meaningful, and deviation of single observations from average results cannot be considered to be variations in the position of the reconnection site.

[55] We estimate the distance to the lobe reconnection site in the Northern Hemisphere using observations near the poleward boundary of the cusp, where the ion distributions show typical D shapes and low-velocity cutoffs are evident in both downgoing and upgoing populations. The results are shown in Figure 14. The horizontal axis is the time and the vertical axis is the calculated distance to

the X line (in the units of R_E). On Figure 14a, we plot the estimated distance along the field line to the X line using observations by SC1 and SC4. The estimated distance is highly variable, from 60 R_E to 10 R_E, which may be a feature of a pulsed reconnection site. Here we would like to note that the estimated distance of 60 R_E corresponds to the time interval 0528–0534 UT, when SC1 is deep inside the cusp. For this time interval the uncertainty of the determination of the distance to the X line might be higher than 50%, as the low-energy cutoffs for both downgoing and upgoing populations are very low. The average distance is ~15 R_E. From the series of SC1, the distance to the reconnection site seems to generally decrease with time. Estimated from SC1 observations, the average speed (obtained by a linear recession) of the reconnection site movement is 0.04 R_E per second, or ~250 km s^{-1}. We refer to this speed as "small-scale speed" since only one cusp crossing is taken into account. The differences of the distances estimated by SC1 and SC4 at the same time visible on Figure 14a are reasonable, since SC4 is nearer to the ionosphere than SC1 when they cross the cusp. On Figure 14b, we plot the estimated distance to the X line for SC3. One hour after SC1 and SC4, the reconnection site estimated from SC3 appears more stable, and the distances remain in the range of 5–15 R_E, generally nearer than that seen by SC1 and SC4. The average distance is ~8 R_E. Here we could estimate the speed of the reconnection site motion in a larger scale, taking into account the difference between the average distance observed by SC1, SC4 and that observed by SC3. The estimated speed is 0.0025 R_E per second, or 16 km s^{-1}. The large-scale speed is one-order smaller than the small-scale speed estimated from SC1 observations, indicating that SC1 observes a fast motion of the reconnection site. The estimated sunward motion of the reconnection site is a somewhat puzzling result. Indeed, computer simulations show that reconnection site in the lobe sector is expected to move antisunward [*Berchem et al.*, 1995; *Omidi et al.*, 1998]. This is explained by the suggestion that in the lobe sector, in the region with super-Alfvénic flow, a reconnection site must move tailward so that the bulk flow speed in the de Hoffman-Teller frame (i.e., frame where the electric field vanishes) is Alfvénic [*Gosling et al.*, 1991]. Further, our observations disagree with observations by *Fuselier et al.* [2000b] of the existence of the stable lobe reconnection site for many minutes under stable solar wind and northward IMF conditions. One possible explanation of the observed sunward displacement of the X line with time is patchy reconnection, when different X lines are formed at different locations. The second possible explanation of the sunward X line motion is a suggestion that magnetosheath plasma flow in the lobe sector is still sub-Alfvénic. From the T96 model, we estimate that the distance along the magnetic field line from the SC3 to the magnetosheath is approximately 4.5 R_E. So the reconnection site is generally not far in the lobe sector of the Northern Hemisphere. The third explanation for the relative distances between the Cluster satellites and the X line at the magnetopause becoming smaller is antisunward motion of the cusp rather than sunward motion of the X line. Thus, field lines that populate the cusp observed by SC3 are located poleward of those observed by SC1, SC2, and SC4, and the distance along these field lines toward the reconnection line might be smaller. The distance between the satellite and position of the X line at the magnetopause also can be influenced by changes in the solar wind dynamic pressure.

4.3. Pulsed Dual Lobe Reconnection

[56] The Cluster satellites cross the northern cusp during the strongly northward and antisunward IMF; these conditions favor the lobe reconnection happening first in the lobe sector of the Northern Hemisphere. On the basis of the common observations by the three spacecraft, e.g., the ions low-energy cutoffs which increase with latitude, downgoing ion populations and sunward convection near the cusp poleward boundary (Figures 3, 5, and 7), indicating the "new" open field lines near the poleward boundary, we propose that the IMF is reconnected with the north lobe of the terrestrial magnetic field first, and the northern lobe reconnection lasts from ~0500 to ~0640 UT, i.e., for more than 100 min. We suggest the following scenario: lobe reconnection is first established in the northern lobe; the open field lines move sunward, drape around the dayside magnetosphere, and may be subsequently reclosed by the secondary reconnection in the Southern Hemisphere. We generally refer this reconnection process as dual lobe reconnection.

[57] For all four cusp crossing events, we observe a region with reduced convection near the equatorward boundary of the cusp, which is characterized by low sunward/antisunward convection. However, duskward-dawnward convection persists as observed on SC1 and SC2. According to *Bogdanova et al.* [2005], the stagnant cusp may be one of the signatures of the dual lobe reconnection. Similar to that study, the observed nearly stagnant cusps are isotropic in terms of ion distribution measured by SC1 and SC4. However, in our case the cusps consist of several short-term transient plasma injections with electron beams, accompanied by the high-energy ions. Some of these electron beams have high energy, and have equal downgoing and upgoing fluxes, especially in the high-energy bands. The bidirectional electron flux is one of the most direct signatures of reclosed field lines [e.g., *Phan et al.*, 2005]. Ion populations with high energy, which correlate with the bidirectional electron beams, suggest that the ions are additionally accelerated. The most plausible explanation of the additional acceleration is the dual lobe reconnection, which provides a second accelerating site in the opposite hemisphere [e.g., *Onsager et al.*, 2001; *Bogdanova et al.*, 2005]. We note that bidirectional electron beams accompanied by these accelerated ions are observed during the periods with low sunward/antisunward convection. Thus, our observations are in contrast to the observations of *Imber et al.* [2006] and *Provan et al.* [2005], which suggest that dual lobe reconnection must be accompanied by sunward flow, and in agreement with observations by *Bogdanova et al.* [2005]. The duskward-dawnward convection observed by SC1 and SC2 might correspond to (1) an initial phase of dual lobe reconnection, when reclosed field lines move according the IMF B_Y sign or (2) a last phase of the dual lobe reconnection process, when reclosed field lines inside the magnetosphere are migrating toward dusk and dawn and being transported from the dayside to the nightside because of interchange instability [e.g., *Song and Russell*, 1992].

Plasma convection inside the cusp observed by SC1, SC2, and SC4 are in agreement with the IMF B_Y sign, and thus these cusps can be on newly reclosed field lines. The duskward-dawnward convection inside the cusp observed by SC3 does not agree with that expected for duskward IMF. This can be an indication that SC3 crosses the cusp on reclosed field lines with some time history since reconnection.

[58] We note that the bidirectional high-energy electron flux and accelerated ions are only observed for short periods inside the region with reduced convection, consistent with only a portion of open field lines created by the first northern lobe reconnection site being reclosed. These pulsed dual lobe reconnection features correspond to flux transfer events (FTEs), whose description is given by *Provan et al.* [2005] and *Sandholt et al.* [2000] on the basis of ionospheric observations. We observe for the first time the occurrence of long-term pulsed dual lobe reconnection uncovered using Cluster multispacecraft facilities.

4.3.1. Electron Azimuthal Cuts Through the Energy Spectra

[59] From the azimuthal cuts through the electron energy spectra, we are able to distinguish the topology of the field lines, in particular when they have been reclosed by dual lobe reconnection.

[60] The most likely periods for the effects of dual lobe reconnection to manifest themselves are those when the spacecraft observe high-energy electron beams and accelerated ion fluxes, e.g., beams b and d for SC1; beams h, i, and j for SC4; and beams o, p, and q for SC3. In Figures 9, 10, and 11, we observe commonly the bidirectional feature in such periods; the fluxes of parallel and antiparallel populations are generally higher than the perpendicular populations for most of the energy range. We note that the parallel and antiparallel populations have balanced fluxes for energies greater than 40 eV and the antiparallel electron flux exceeds the parallel one at the low-energy (10–40 eV) bin. The additional antiparallel electron flux is likely due to the outflow from the ionosphere and should not undermine the general bidirectional properties.

[61] In comparison with the 2-D cuts of the electron energy spectra near the poleward boundary, where the field lines are open, we may conclude that the field lines on which we observe bidirectional electron fluxes are reclosed and have undergone dual lobe reconnection. If the field line is open, the counterstreaming populations are not balanced, which are the case in the last example on Figures 9, 10, and 11. Finally we confirm that the bidirectional electron flux is a signature of the dual lobe reconnection, and the high-energy electron and ion beams we observe above are due to the dual lobe reconnection that the field lines have undergone.

[62] We note that in the case of SC3, the electron beams are not bidirectional in all energy bins. We still consider the electron beams that are bidirectional in high-energy end to be due to the dual lobe reconnection for the following reasons: (1) electrons mostly affected by the dual lobe reconnection are those with high energy, since the secondary reconnection accelerates the electrons to higher energy, and (2) balance of the downgoing and upgoing electrons may not be detected in low-energy bands because pulsed dual lobe reconnection occurs so rapidly that the electrons do not have sufficient time to become balanced.

4.3.2. Periodicity of Dual Lobe Reconnection

[63] Now we summarize the method used to determine the reclosed field lines. Our criteria on plasma properties are high-energy populations for electrons and ions [e.g., *Onsager et al.*, 2001; *Bogdanova et al.*, 2005] and the bidirectional properties revealed by the azimuthal cuts through the electron energy spectra [e.g., *Phan et al.*, 2005]. On the basis of these criteria we could determine the specific periods where the spacecraft cross the reclosed field lines for the whole event, which provide the possibility to estimate the periodicity of the pulsed dual lobe reconnection.

[64] Our approach in the determination of reclosed field lines and possible dual lobe reconnection, which is based on the observations of plasma properties by the Cluster satellites, has an obvious advantage in time resolution in comparison with ionospheric observations. As the ionospheric observations have relatively low time resolution (the latest SuperDARN radar instruments do one complete high-latitude ionosphere survey every two minutes), some short-term dual reconnection processes, even the pulsed feature as a whole, might be missed.

[65] With our approach to identify the occurrence of dual lobe reconnection, we are able to estimate its periodicity. As we reported above, the spacecraft sample open and reclosed field lines alternatively, and, investigating electron spectra with 4 s resolution, we can say that the electron population is highly variable from one spin to another. Nevertheless, we can find the balanced counterstreaming population which last for a few spins inside the beams b and d for SC1; beams h, i, and j for SC4; and beams o, p, and q for SC3. Taking into account the times between separate beams, we deduce the periodicity of dual lobe reconnection to be variable between 1 and 5 min. These observations are similar to the periodicity of dual reconnection reported by *Bogdanova et al.* [2007], which was estimated to be $\sim$1 min. However, our estimation of the periodicity of dual reconnection is much lower than that estimated by *Provan et al.* [2005] using SuperDARN data, which was $\sim$15 min. However, as we pointed out before, this disagreement could be due to the different time resolution, as Cluster observes small-scale structure of plasma injections which are missed by SuperDARN observations.

[66] We note that the determined periodicity of the reconnection pulses is based on the observational signatures. The relevance between the observational signatures and the actual reconnection process may result in the following effects: (1) the reconnection pulses may actually last longer than we estimate, (2) the pulses we observe may also be due to different reconnection sites, and (3) the time of observation depends also on the relative motion of the spacecraft and field lines. Bearing in mind the limit of this estimation, we still believe that the estimation gives a reasonable value of the periodicity of reconnection pulses. We roughly estimated the propagation time of the electrons from the secondary lobe reconnection site to the spacecraft to be a few seconds. So the actual happening time of the secondary lobe reconnection is several seconds before the observational time. Additionally, the propagation time of the ions accelerated at the reconnection site in the Southern Hemisphere is longer, around 5 min.

4.3.3. Ion Distributions

[67] We examine the ion distributions in order to better understand the H^+ ions behavior along reclosed and open field lines. In Figures 9 and 10, the properties of the ion distributions are clearly different for the reclosed field lines and the new open field lines, in the case of SC1 and SC4 cusp crossings. The ion distributions are isotropic along the reclosed field lines, indicated by the "round" distributions and the similar cross sections. From the scenario we suggest above, the reclosed field lines are "old" field lines in respect to the first reconnection, therefore ions have been scattered sufficiently, and the more isotropic distributions are formed. Near the cusp poleward boundary, however, ions propagating parallel to the local field line are dominant, which is indicated by the single D-shaped distributions and higher $V_{perp} = 0$ cross sections (right columns of Figures 9, 10, and 11). Here the spacecraft cross the new open field lines generated by the northern lobe reconnection so that the ions show injection properties [e.g., *Smith and Lockwood*, 1996]. From the comparison of the ion distributions between reclosed field lines and open field lines, we may conclude that the ion distributions tend to be more isotropic if the field lines are reclosed. However, we note that the isotropic ion distributions are commonly observed on the open field lines with some time history since reconnection [e.g., *Smith and Lockwood*, 1996]. So this signature is not a unique feature of the dual lobe reconnection and the reclosed field lines.

[68] Ion distributions inside the cusp observed on SC3 are different to those detected on SC1 and SC4. Indeed, SC3 does not cross any field lines with quasi-isotropic ion distributions. A number of factors can be responsible for such observations. Here we suggest two simple explanations. First, it is possible that the reconnection process is pulsed with a high repetition rate during the time interval when SC3 crosses the cusp, and thus SC3 is nearly always crossing newly reconnected field lines where the mirroring population has not developed yet. Second, this might be an effect of the closeness of the X line: again, because of a shorter time of flight of magnetosheath-like particles from the reconnection line to the satellite to those observed by SC1 and SC4, it is possible that the mirroring population does not have enough time to develop. More complicated explanations, involving both spatial and temporal effects, are possible, but this is beyond of the scope of this paper.

[69] We have also investigated the O^+ ion distributions for the periods where the dual lobe reconnection signatures are observed. If the field line is reclosed in the other hemisphere, O^+ ions, which are originated in the ionosphere, will be outflowing along magnetic field lines from the southern ionosphere and may be observed as a downgoing population in the northern cusp [*Fuselier et al.*, 2001]. We do not observe downgoing O^+ ions in our events. The flight time of the O^+ ions from the southern ionosphere to the spacecraft is several minutes, but the periodicity of the dual reconnection is $\sim$1 min, so we propose that O^+ do not have sufficient time to reach the spacecraft. There are other explanations as to why Cluster does not observe downgoing O^+ ions during this event. The simplest explanation is that there are no upflowing ionospheric heavy ions in the Southern Hemisphere on these field lines. Also the energy of the O^+ ions may not be sufficient to be detected with the CODIF instrument. Thus, *Sauvaud et al.* [2001] showed that the O^+ ions could be seen at the magnetopause only because of the magnetopause motion. If there is no magnetopause motion the O^+ ions may not be energized enough to be detected when they enter the cusp.

4.4. Features on the Cusp Equatorward Boundary

[70] In the multispacecraft observations we report, the plasma features near the cusp equatorward boundary are different between the three spacecraft (SC1, SC3, and SC4) crossings. We now discuss these special features and suggest some explanations. This may help us to understand the mechanism of the lobe reconnection, especially the establishment phase after the IMF orientation changes from southward to northward.

[71] SC1 observes a separate plasma population near the equatorward boundary of the cusp (Figure 3). This population has properties consistent with formation by the dayside subsolar reconnection properties, such as low-energy cutoffs which decrease with latitude and the antisunward convection. These field lines are thus residue of the previous dayside reconnection. This observation suggests that immediately after the IMF rotation, the previous open field lines will continue to be present near the cusp equatorward boundary. The lifetime of these field lines can be estimated from our observations. When SC1 reenters the cusp at $\sim$0504 UT, it continues to cross the field lines originated from dayside reconnection till $\sim$0508 UT. The lifetime of the open field lines after the IMF rotation in our case is estimated to be $\sim$10 min. The short-term switch off after the separate population may be due to the rapid movement of the whole cusp. As the solar wind dynamic pressure increases suddenly, the cusp can be driven antisunward so quickly that the spacecraft moves outside the cusp for a short period [*Eastman et al.*, 2000]. Observations of the convection velocity support this suggestion. One short-term negative peak of the X component of the perpendicular velocity at this time may be due to the antisunward movement of the whole cusp. Another possible explanation of this motion is the reaction of the cusp on the IMF northward turning, as illustrated in the case study by *Pitout et al.* [2006] and in the statistical study by *Newell et al.* [2006].

[72] SC4 enters the cusp when the lobe reconnection has been established, so that it observes a sharp equatorward boundary of the cusp (Figure 5). Once it enters the cusp, it crosses the nearly stagnant part on field lines which have undergone dual lobe reconnection.

[73] SC3 enters the cusp when the lobe reconnection has been established for more than 1 h. It should have detected a sharp equatorward boundary as did SC4. However, it observes a separate plasma population near the cusp equatorward boundary. Moreover, the separate population has low-energy cutoffs decreasing with latitude (Figure 7), which are thought to be the signature of dayside reconnection. But it is very unlikely that dayside reconnection happens during long-term northward IMF. Further, as long as northern lobe reconnection has been established for more than 1 h, this short-term population should be a pure lobe reconnection phenomenon. This separate population has sunward and dawnward convection. Note that the nearly stagnant part of the cusp has duskward convection.

Table 2. Result of the Events Survey in the Summer and Autumn 2004 and 2005[a]

Clock Angle	0–10°	10–20°	20–30°	30–40°	40–50°	>50°
Number of events	1	1	3	4	7	6

[a]The second row shows the number of events whose IMF clock angles are in the range indicated in the first row.

[74] For a cusp formed by plasma injections from the single lobe reconnection process, near the boundary far from the reconnection site, the distributions are expected to show a mixture of population mirrored from the ionosphere and the precipitating population. Since there are no isotropic mirrored populations in this interval, it is not a typical single lobe reconnection cusp crossing. As discussed before, one possible explanation is that SC3 crosses always "newly" reconnected field lines in the Northern Hemisphere, on which the mirroring ion population is not developed sufficiently. Thus, these observations can suggest that, as observed on SC3, if dual lobe reconnection takes place, the reconnection process occurs nearly simultaneously in both hemispheres. This is in agreement with the observations of the multiple positive velocity cutoffs. As shown in Figure 12, the double D-shaped populations indicate independent injections, possibly accelerated by two reconnection sites. Moreover, sudden directional change of the Y component of perpendicular velocity at ~0605 UT might suggest that the spacecraft crosses field lines dominated by the reconnection in the Southern Hemisphere to the field lines dominated by the reconnection in the Northern Hemisphere. We also suggest that the plasma injections from different reconnection sites may have different convection in the duskward-dawnward direction. The second subinterval (0605–0608 UT) may be the transitional phase between dual lobe reconnection and single lobe reconnection.

[75] However, the energy of this separate population near the equatorward boundary of the cusp is much lower than that inside the nearly stagnant cusp. The lack of the high energy, additionally accelerated, ions and the bidirectional electrons contradicts the explanation that these injections are produced by the dual lobe reconnection. There are other possible explanations for the double distinct injections suggested by the double low-velocity cutoffs. One may suggest that the high-energy D-shaped population in Figure 12 is actually precipitating plasma sheet ions. However, the plasma sheet-like ions shown in Figure 7 have energies of about 10 keV, corresponding to the velocities of about 1400 km s^{-1}, which are much higher than the second velocity cutoff observed in the H^+ ions distribution functions. Thus, we report here very interesting observations of the plasma population inside the cusp observed on SC3, and interpretation of this part is a subject of future work.

5. A Statistical Study: Stagnant Cusp, Dual Lobe Reconnection, and Northward IMF

[76] In the presented study, the nearly stagnant cusp, or region with reduced convection, is commonly observed in the case of dual lobe reconnection. As the field lines near the equatorward boundary of cusp are reclosed by dual lobe reconnection and stop moving, the newly opened field lines might be accumulated in the cusp and thus they should not have a high convection speed; some of them are possibly reclosed by the reconnection processes on the opposite hemisphere. *Bogdanova et al.* [2005] reported a case study indicating that stable dual lobe reconnection may generate a stagnant and isotropic cusp. The case reported here further indicates that the pulsed dual lobe reconnections may generate a nearly stagnant cusp, but not necessarily isotropic. However, there is a controversy about the IMF conditions favorable for dual lobe reconnection. Some studies suggest that the dual lobe reconnection can only occur under strongly northward IMF (CA < 10°) [*Imber et al.*, 2006]. To find the dependency between the stagnant cusp observations, occurrence of dual lobe reconnection and the IMF clock angle, we perform a general survey of all Cluster midaltitude cusp crossing events from July to October, years 2004 and 2005. Only the events when IMF has a northward component are chosen. Overall, there are 22 midaltitude cusp crossings during northward IMF in 2004 and 2005.

[77] We group the events in six groups according to the IMF clock angle, as shown in Table 2. Events with small clock angle are very rare. We choose randomly one event from each group and investigate the plasma convection of these events. For all these example events, we analyze the convection velocity inside the cusp and for all events find the stagnant region inside it. The criterion for the cusp to be stagnant is the convection velocity less than 10 km s^{-1}. We note that the error limit of the ion bulk velocity measurement by CIS instrument is ±5 km s^{-1}. We use mainly the X component of the perpendicular velocity as the indicator of the convection velocity, as it shows the sunward (antisunward) movements of the magnetic field lines. However, we should remember that the Y component of the perpendicular velocity may be more important than the X component when the IMF has a large clock angle.

[78] Since it has been suggested that dual lobe reconnection can only occur during strongly northward IMF, it is surprising to find that the stagnant cusp, one of the suggested possible signatures of the dual lobe reconnection, occurs commonly under the IMF with the CA between 40° and 60°. To reveal the relation between stagnant cusps and the IMF conditions, we study the cusp crossing events from July to early October 2004 and 2005 when the IMF clock angles are between 40 and 60°. There are 13 such events from the event survey (Table 2) and 9 cusp crossing events studied. For the other 4 events we do not have clear PEACE and CIS data coverage. The principle descriptions of the events are gathered in Table 3. Each row shows one event. The first three columns show the date of event; the fourth column indicates the spacecraft of observations; the fifth, sixth and seventh columns show the time and duration of the cusp crossing; the eighth column shows the IMF clock angle; the ninth column shows the duration of crossing of the cusp stagnant part determined by taking into account the X and Y components of the perpendicular velocity; the tenth column shows the "stagnation ratio," which is defined to be the ratio between the duration of the stagnant cusp and the duration of the entire cusp crossing; and the last column gives main features of events.

Table 3. Summary of Properties of the Events Whose IMF Clock Angles are Between 40° and 60° in the Summer and Autumn 2004 and 2005[a]

Year	Month	Date	SC	Cusp Crossing From (UT)	Cusp Crossing To (UT)	Duration of Cusp Crossing (min)	CA (degrees)	Duration of Stagnant Cusp Crossing (min)	Stagnation Ratio	Main Features
2004	7	16	3	1203	1222	19	50–60	6	0.316	two stagnant parts
2004	8	4	1	1641	1659	18	40–50	15	0.833	two injections and two stagnant parts
2004	9	6	1	1830	1907	37	40–50	29	0.784	...
2004	9	16	1	0740	0820	40	40–50	28	0.7	multiple very short injections
2004	9	18	1	1554	1630	36	50–60	20	0.556	very low convection during injections
2004	9	18	1	2117	2220	63	40–50	28	0.444	very low convection during injections
2004	10	3	1	0414	0433	19	50–60	0	0	very unstable
2005	9	21	3	0221	0248	27	50–60	12	0.444	very low convection during injections
2005	9	30	3	1352	1409	17	40–50	13	0.765	dayside reconnection

[a]The stagnation ratio is defined as the ratio between the duration of the whole cusp crossing and the duration of the stagnant cusp crossing.

[79] All events with 40–50° IMF CA have the signatures of the stagnant cusp. The average duration of the stagnant cusp crossing for these events is 22.6 min, and the average stagnation ratio is 0.64. We can assert that a major part of the cusp is stagnant under the IMF with a CA of 40–50°. There are some other features appearing, such as multiple injections. We believe that it might be related to fluctuations of the IMF. Note that one of the studied cusp crossing events on 30 September 2005 can be explained by the plasma injections from the dayside reconnection, as there are plasma injections at the equatorward boundary of the cusp, and normal energy-time dispersion. Still, a region with stagnant plasma is observed.

[80] Events with the IMF CA of 50–60° have more complicated properties. Except for one cusp with highly unstable injections, the rest have a stagnant part. The average duration of the stagnant cusp crossing for these events is 9.5 min, and the average stagnation ratio is 0.33. We note that the stagnant cusps are much less likely for these IMF conditions. For some events, we observe the very low convection velocity (less than 10 km s^{-1}) even near the poleward boundary, which makes it difficult to distinguish the stagnant cusp. Our observations agree with previous statistical study by *Lavraud et al.* [2005] that stagnation of the plasma flow inside the cusp is a common signature during northward IMF. However, because of studying the convection dependency from the IMF clock angle, we are able to conclude that stagnation of the flow is more common for the IMF with the CA ~40–50° than with the CA ~50–60°.

[81] It has been suggested that dual lobe reconnection can only occur during strongly northward IMF [*Imber et al.*, 2006], e.g., when the IMF clock angle is <10°. So the results of this study give us two possible explanations: dual lobe reconnection can happen for more broad range of the northward IMF clock angles (this is in agreement with *Lavraud et al.* [2006]); or the stagnant cusp is not a unique signature of dual lobe reconnection. In this study, the short period of stagnation inside the cusp is observed for the events with the IMF clock angle more than 50°, when the B_Y component dominates, for which dual lobe reconnection is not likely to happen. Thus, there might be other mechanisms to explain the stagnation of the plasma flow during dawnward and duskward IMF. However, we note that although stagnation is observed for different IMF CA, the stagnation ratio is higher in the low IMF CA cases than that in the high IMF CA cases.

6. Conclusions

[82] In this paper we report a case study based on Cluster multispacecraft observations. Our observations have advantages in three perspectives: (1) stable low clock angle of the IMF during the entire event, (2) long-term observations by the satellites crossing the cusp successively, and (3) possibility to study the establishment of the lobe reconnection because SC1 covers the transitional phase, and SC4 and SC3 covers the stable phase. Analyzing plasma population inside the cusp, we conclude that the pulsed dual lobe reconnection process forms some parts of the cusp. We concentrate on the analysis of the following signatures inside the cusp, assuming that they are signatures of dual lobe reconnection: (1) cusp stagnation, indicated by low convection velocity; (2) counterstreaming electrons with equal fluxes in the parallel and antiparallel directions at all energies; and (3) magnetosheath-like ions with high energy. We study the ion distributions and conclude that the isotropic ions distribution might also be a signature of the dual lobe reconnection. We note however that it is not a unique signature of dual lobe reconnection, as the isotropic ion distribution can exist on the open field lines with some history since reconnection, when the downgoing population still exists and upgoing population is already well developed. We determine the periods when the spacecraft cross reclosed field lines and estimate the periodicity of the reconnection pulse to be ~1–5 min. SC1 and SC4 observe regular reconnection pulses. In this study, field lines formed by the dual lobe reconnection are nearly stagnant. Thanks to the multispacecraft observations, we estimate the motion of the cusp boundaries and variations in the cusp size. In the transitional phase immediately after the IMF turning from southward to northward orientation, the cusp size decreases rapidly. In the stable phase, when dual lobe reconnection is ongoing, the cusp size expands gradually at the speed of

Table 4. Summary of Observational Signatures of Pulsed Dual Lobe Reconnection[a]

	Signatures of Pulsed Dual Lobe Reconnection Inside the Cusp
1	Quasi-periodic enhancements in the plasma flux and density
2	Equal fluxes of counterstreaming magnetosheath-like electrons, especially at higher energies, $E > 200$ eV
3	Quasi-periodic enhancements of fluxes of the ion population with energies $E > 5$ keV
4	Reduced convection inside the cusp
5	Periodicity is 1–5 minutes
6	Both the high- and low-latitude boundaries of the cusp move poleward
7	The size of the cusp increases with time at a rate of 0.5° ILAT per hour

[a]As observed by the 1210 Cluster satellites inside the midaltitude cusp.

0.4° ILAT per hour. The observational signatures of pulsed dual lobe reconnection deduced in this study are summarized in Table 4. We estimate the distance from each spacecraft to the lobe reconnection site in the Northern Hemisphere and its variation with time. In the transitional phase, the reconnection site is unstable and generally moves sunward at the speed of 254 km s^{-1} while in a large scale, the reconnection site moves sunward at the speed of 16 km s^{-1}. Thus, we observe a fast motion of the reconnection site during the transitional phase. In the stable phase, the reconnection site is around 8 R_E from the spacecraft. From another perspective, SC3 observations show special features: (1) separate injections with normal energy-time dispersion near the equatorward boundary, (2) abnormal dawnward/duskward convection in the nearly stagnant cusp, (3) anisotropic ions along the presumably reclosed field lines, and (4) quasiperiodic reconnection pulses. The analysis of these observations will be a subject of further study. Finally, to reveal the relation between the stagnation of plasma flow inside the cusp, the occurrence of the dual lobe reconnection process and the northward IMF, we study the convection inside the midaltitude cusp region under northward IMF over 2 years, 2004 and 2005, in a statistical way. The plasma stagnation inside the cusp is observed for different IMF CA and commonly observed during the IMF clock angle ~40–60°. This suggests that the stagnation of the flow might not be a unique signature of the dual lobe reconnection process. However, we note that the duration of stagnation is longer for the events with lower clock angle.

[83] **Acknowledgments.** R.H. is sponsored by the Dean's Summer Studentship of University College London, United Kingdom, and by the National Natural Science Foundation of China (NSFC) grant 10533020 and Ministry of Education SRFDP 20050003088 at Tsinghua University, China. Y.V.B., C.J.O., C.F., and A.N.F. are supported by MSSL STFC Rolling Grant. We are thankful to I.V. Alexeev for fruitful discussion. We thank the Operation Teams of the PEACE, FGM, and CIS instruments for the Cluster data. We thank CDAweb for the ACE data and the OVT team for providing Cluster orbit plots.

[84] Amitava Bhattacharjee thanks Christopher Philippe Escoubet and another reviewer for their assistance in evaluating this manuscript.

References

Balogh, A., et al. (2001), The Cluster Magnetic Field Investigation: Overview of in-flight performance and initial results, *Ann. Geophys.*, *19*, 1207–1217.

Berchem, J., J. Raeder, and M. Ashour-Abdalla (1995), Magnetic flux ropes at the high-latitude magnetopause, *Geophys. Res. Lett.*, *22*(10), 1189–1192, doi:10.1029/95GL01014.

Bogdanova, Y. V., A. Marchaudon, C. J. Owen, M. W. Dunlop, H. U. Frey, J. A. Wild, A. N. Fazakerley, B. Klecker, J. A. Davies, and S. E. Milan (2005), On the formation of the high-altitude stagnant cusp: Cluster observations, *Geophys. Res. Lett.*, *32*, L12101, doi:10.1029/2005GL022813.

Bogdanova, Y. V., C. J. Owen, A. N. Fazakerley, B. Klecker, and H. Reme (2006), Statistical study of the location and size of the electron edge of the low-latitude boundary layer as observed by Cluster at mid-altitudes, *Ann. Geophys.*, *24*, 2645–2665.

Bogdanova, Y. V., C. J. Owen, G. Siscoe, A. N. Fazakerley, I. Dandouras, O. Marghitu, Z. Kaymaz, H. Reme, and E. A. Lucek (2007), Cluster observations of the magnetospheric low-latitude boundary layer and cusp during extreme solar wind and interplanetary magnetic field conditions: part II. 7 November 2004 ICME and statistical survey, *Sol. Phys.*, doi:10.1007/s11207-007-0418-0.

Burch, J. L., P. H. Reiff, R. W. Spiro, R. A. Heelis, and S. A. Fields (1980), Cusp region particle precipitation and ion convection for northward interplanetary magnetic field, *Geophys. Res. Lett.*, *7*(5), 393–396, doi:10.1029/GL007i005p00393.

Cowley, S. W. H. (1983), Interpretation of observed relationships between solar wind characteristics and effects at ionospheric altitudes, in *High Latitude Space Plasma Physics*, edited by B. Hultqvist and T. Hagfors, pp. 225–249, Plenum, New York.

Crooker, N. U. (1979), Dayside merging and cusp geometry, *J. Geophys. Res.*, *84*, 951–959, doi:10.1029/JA084iA03p00951.

Dungey, J. W. (1961), Interplanetary magnetic field and the auroral zones, *Phys. Rev. Lett.*, *6*, 47–48, doi:10.1103/PhysRevLett.6.47.

Dungey, J. W. (1963), The structure of the ionosphere, or adventures in velocity space, in *Geophysics: The Earth's Environment*, edited by C. Dewitt, J. Hieblot, and A. Lebeau, 505 pp., Gordon and Breach, New York.

Eastman, T. E., S. A. Boardsen, S.-H. Chen, S. F. Fung, and R. L. Kessel (2000), Configuration of high-latitude and high-altitude boundary layers, *J. Geophys. Res.*, *105*, 23,221–23,238, doi:10.1029/1999JA900269.

Escoubet, C. P., M. Fehringer, and M. Goldstein (2001), The Cluster mission, *Ann. Geophys.*, *19*, 1197–1200.

Frey, H. U., S. B. Mende, T. J. Immel, S. A. Fuselier, E. S. Claflin, J.-C. Gérard, and B. Hubert (2002), Proton aurora in the cusp, *J. Geophys. Res.*, *107*(A2), 1091, doi:10.1029/2001JA900161.

Fuselier, S. A., K.-J. Trattner, and S. M. Petrinec (2000a), Cusp observations of high- and low-latitude reconnection for northward interplanetary magnetic field, *J. Geophys. Res.*, *105*, 253–266, doi:10.1029/1999JA900422.

Fuselier, S. A., S. M. Petrinec, and K.-J. Trattner (2000b), Stability of the high-latitude reconnection site for steady northward IMF, *Geophys. Res. Lett.*, *27*, 473–476, doi:10.1029/1999GL003706.

Fuselier, S. A., S. M. Petrinec, K. J. Trattner, and W. K. Peterson (2001), O^+ observations in the cusp: Implications for dayside magnetic field topology, *J. Geophys. Res.*, *106*, 5977–5986, doi:10.1029/2000JA003030.

Gosling, J. T., M. F. Thomsen, S. J. Bame, R. C. Elphic, and C. T. Russell (1991), Observations of reconnection of interplanetar and lobe magnetic field lines at the high-latitude magnetopause, *J. Geophys. Res.*, *96*, 14,097–14,106, doi:10.1029/91JA01139.

Gustafsson, G., et al. (2001), First results of electric field and density observations by Cluster EFW based on initial months of operation, *Ann. Geophys.*, *19*, 1219–1240.

Imber, S. M., S. E. Milan, and B. Hubert (2006), The auroral and ionospheric flow signatures of dual lobe reconnection, *Ann. Geophys.*, *24*, 3115–3129.

Johnstone, A. D., et al. (1997), Peace: A plasma electron and current experiment, *Space Sci. Rev.*, *79*, 351–398, doi:10.1023/A:1004938001388.

Lavraud, B., A. Fedorov, E. Budnik, M. F. Thomsen, A. Grigoriev, P. J. Cargill, M. W. Dunlop, H. Rème, I. Dandouras, and A. Balogh (2005), High-altitude cusp flow dependence on IMF orientation: A 3-year Cluster statistical study, *J. Geophys. Res.*, *110*, A02209, doi:10.1029/2004JA010804.

Lavraud, B., M. F. Thomsen, B. Lefebvre, S. J. Schwartz, K. Seki, T. D. Phan, Y. L. Wang, A. Fazakerley, H. Rème, and A. Balogh (2006), Evidence for newly closed magnetosheath field lines at the dayside magnetopause under northward IMF, *J. Geophys. Res.*, *111*, A05211, doi:10.1029/2005JA011266.

Lockwood, M., and M. F. Smith (1994), Low and middle altitude cusp particle signatures for general magnetopause reconnection rate variations: 1. Theory, *J. Geophys. Res.*, *99*, 8531–8554, doi:10.1029/93JA03399.

McComas, D. J., S. J. Bame, P. Barker, W. C. Feldman, J. L. Phillips, P. Riley, and J. W. Griffee (1998), Solar Wind Electron Proton Alpha Monitor (SWEPAM) for the Advanced Composition Explorer, *Space Sci. Rev.*, *86*, 563–612, doi:10.1023/A:1005040232597.

Newell, P. T., and C.-I. Meng (1994), Ionospheric projections of magnetospheric regions under low and high solar wind pressure conditions, *J. Geophys. Res.*, *99*, 273–286, doi:10.1029/93JA02273.

Newell, P. T., T. Sotirelis, K. Liou, C. I. Meng, and F. J. Rich (2006), Cusp latitude and the optimal solar wind coupling function, *J. Geophys. Res.*, *111*, A09207, doi:10.1029/2006JA011731.

Omidi, N., H. Karimabadi, and D. Krauss-Varban (1998), Hybrid simulation of the curved dayside magnetopause during southward IMF, *Geophys. Res. Lett.*, *25*, 3273–3276, doi:10.1029/98GL02484.

Onsager, T. G., J. D. Scudder, M. Lockwood, and C. T. Russell (2001), Reconnection at the high-latitude magnetopause during northward interplanetary magnetic field conditions, *J. Geophys. Res.*, *106*(A11), 25,467–25,488, doi:10.1029/2000JA000444.

Phan, T.-D., M. Oieroset, and M. Fujimoto (2005), Reconnection at the dayside low-latitude magnetopause and its nonrole in low-latitude boundary layer formation during northward interplanetary magnetic field, *Geophys. Res. Lett.*, *32*, L17101, doi:10.1029/2005GL023355.

Pitout, F., C. P. Escoubet, Y. V. Bogdanova, E. Georgescu, A. N. Fazakerley, and H. Rème (2006), Response of the mid-altitude cusp to rapid rotations of the IMF, *Geophys. Res. Lett.*, *33*, L11107, doi:10.1029/2005GL025460.

Provan, G., M. Lester, A. Grocott, and S. W. H. Cowley (2005), Pulsed flows observed during an interval of prolonged northward IMF, *Ann. Geophys.*, *23*, 1207–1225.

Reiff, P. H., R. W. Spiro, and J. L. Burch (1980), Cusp proton signatures and the interplanetary magnetic field, *J. Geophys. Res.*, *85*, 5997–6005, doi:10.1029/JA085iA11p05997.

Rème, H., et al. (2001), First multispacecraft ion measurements in and near the Earth's magnetosphere with the identical Cluster Ion Spectrometry (CIS) experiment, *Ann. Geophys.*, *19*, 1303–1354.

Sandholt, P. E., C. J. Farrugia, S. W. H. Cowley, M. Lester, W. F. Denig, J.-C. Cerisier, S. E. Milan, J. Moen, E. Trondsen, and B. Lybekk (2000), Dynamic cusp aurora and associated pulsed reverse convection during northward interplanetary magnetic field, *J. Geophys. Res.*, *105*, 12,869–12,894, doi:10.1029/2000JA900025.

Sauvaud, J.-A., et al. (2001), Intermittent thermal plasma acceleration linked to sporadic motions of the magnetopause, first Cluster results, *Ann. Geophys.*, *19*, 1523–1532.

Smith, C. W., J. L'Heureux, N. F. Ness, M. H. Acuña, L. F. Burlaga, and J. Scheifele (1998), The ACE magnetic fields experiment, *Space Sci. Rev.*, *86*, 613–632, doi:10.1023/A:1005092216668.

Smith, M. F., and M. Lockwood (1996), Earth's magnetospheric cusps, *Rev. Geophys.*, *34*, 233–260, doi:10.1029/96RG00893.

Song, P., and C. T. Russell (1992), Model of the formation of the low-latitude boundary layer for strongly northward interplanetary magnetic field, *J. Geophys. Res.*, *97*, 1411–1420, doi:10.1029/91JA02377.

Trattner, K. J., S. A. Fuselier, W. K. Peterson, and C. W. Carlson (2002), Spatial features observed in the cusp under steady solar wind conditions, *J. Geophys. Res.*, *107*(A10), 1288, doi:10.1029/2001JA000262.

Trattner, K. J., S. A. Fuselier, and S. M. Petrinec (2004), Location of the reconnection line for northward interplanetary magnetic field, *J. Geophys. Res.*, *109*, A03219, doi:10.1029/2003JA009975.

Trattner, K. J., S. M. Petrinec, W. K. Peterson, S. A. Fuselier, and H. Reme (2006), Tracing the location of the reconnection site from the northern and southern cusps, *J. Geophys. Res.*, *111*, A11211, doi:10.1029/2006JA011673.

Tsyganenko, N. A. (1995), Modeling the Earth's magnetospheric magnetic field confined within a realistic magnetopause, *J. Geophys. Res.*, *100*, 5599–5612, doi:10.1029/94JA03193.

Twitty, C., T. D. Phan, G. Paschmann, B. Lavraud, H. Rème, and M. Dunlop (2004), Cluster survey of cusp reconnection and its IMF dependence, *Geophys. Res. Lett.*, *31*, L19808, doi:10.1029/2004GL020646.

Vontrat-Reberac, A., J. M. Bosqued, M. G. G. T. Taylor, B. Lavraud, D. Fontaine, M. W. Dunlop, H. Laakso, N. Cornilleau-Werhlin, P. Canu, and A. Fazakerley (2003), Cluster observations of the high-altitude cusp for northward interplanetary magnetic field: A case study, *J. Geophys. Res.*, *108*(A9), 1346, doi:10.1029/2002JA009717.

Weimer, D. R., D. M. Ober, N. C. Maynard, M. R. Collier, D. J. McComas, N. F. Ness, C. W. Smith, and J. Watermann (2003), Predicting interplanetary magnetic field (IMF) propagation delay times using the minimum variance technique, *J. Geophys. Res.*, *108*(A1), 1026, doi:10.1029/2002JA009405.

Zhou, X. W., C. T. Russell, G. Le, S. A. Fuselier, and J. D. Scudder (2000), Solar wind control of the polar cusp at high altitude, *J. Geophys. Res.*, *105*, 245–252, doi:10.1029/1999JA900412.

Y. V. Bogdanova, Department of Physics, La Trobe University, Melbourne, Vic 3086, Australia. (y.bogdanova@latrobe.edu.au)

A. N. Fazakerley, C. Foullon, and C. J. Owen, Mullard Space Science Laboratory, University College London, Dorking RH5 6NT, UK.

R. Hu, Tsinghua Centre for Astrophysics, Department of Physics, Tsinghua University, Haidian District, 100084 Beijing, China.

H. Rème, Centre d'Etude Spatiale des Rayonnements, Centre National de la Recherche Scientifique, 9 Avenue du Colonel Roche, F-31028 Toulouse, France.